

High-order accurate spectral elements for wave problems

Lonny L. Thompson* Sunil K. Challa†

Computational Mechanics Laboratory
Clemson University

Technical Report CMCU-98-03

August 1998

*Assistant Professor of Mechanical Engineering and Engineering Mechanics, Computational Mechanics Laboratory, Clemson University, Clemson, SC, 29634 (USA).

†Graduate Research Assistant, Department of Mechanical Engineering, Clemson University, Clemson, SC. 29634 (USA).

Abstract

In order to accurately resolve waves governed by the Helmholtz equation, the standard low-order Galerkin finite elements with piecewise linear approximation require at least ten elements per wavelength. For large frequencies, accurately resolving the resulting small acoustic wavelengths may lead to prohibitive computational cost in both memory and solution times. Furthermore, a global pollution error increases with increasing wavenumber, even when the number of elements per wavelength is held constant. In this work, spectral elements (both linear and quadratic approximations) are developed which significantly reduce both local approximation (dispersion) error and global pollution effects. The elements employ optimally selected quadrature points and associated weighting parameters for the numerical integration of the element arrays emanating from the discretization of the Galerkin form of the Helmholtz problem. The resulting dynamic stiffness arrays vary only as linear combinations with respect to frequency, and therefore can be used for the corresponding direct time-domain solution of the wave equation. Numerical comparisons with Galerkin and Generalized Galerkin finite elements, and finite-difference methods, show greatly improved accuracy with corresponding reduction in pollution.

HIGH-ORDER ACCURATE SPECTRAL ELEMENTS
FOR WAVE PROPAGATION PROBLEMS

A Thesis
Presented to
The Graduate School of
Clemson University

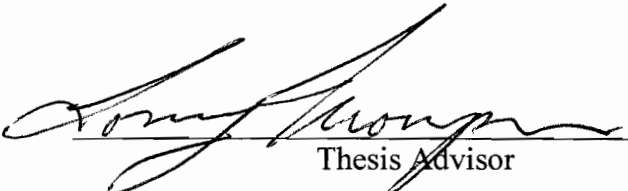
In Partial Fulfillment
Of the Requirements for the Degree
Master of Science
Engineering Mechanics

by
Sunil K. Challa
August 1998

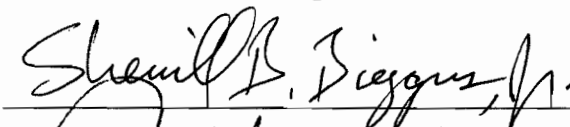
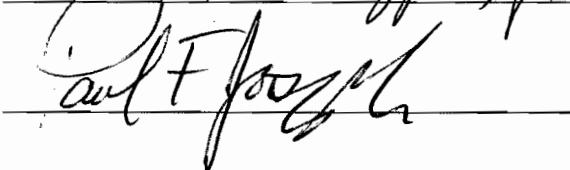
August 3, 1998

To the Graduate School:

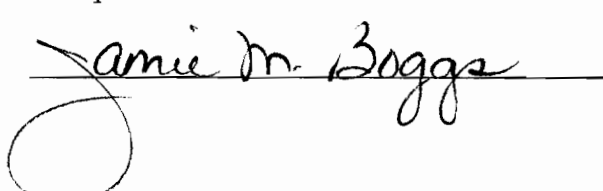
This thesis entitled "High-Order Accurate Spectral Elements for Wave Propagation Problems" and written by Sunil Kumar Challa is presented to the Graduate School of Clemson University. I recommend that it be accepted in partial fulfillment of the requirements for the degree of Master of Science with a major in Engineering Mechanics.


Thesis Advisor

We have reviewed this thesis
and recommend its acceptance:

Accepted for the Graduate School:



ABSTRACT

In order to accurately simulate wave propagation using the standard Galerkin finite element method, several elements per wavelength are required. In the frequency domain, solutions exhibit a pollution effect from boundary conditions in which the error increases with wavenumber even as the elements per wavelength remains constant. In this work we develop a new spectral element method which is designed to reduce dispersion error and to minimize the pollution effect in multi-dimensions. The method employs optimal quadrature points and associated weighting for both stiffness and mass arrays obtained from a condition which minimizes dispersion. The resulting spectral element arrays are frequency independent and therefore can be used for both time-harmonic and transient solutions. Numerical comparisons with various Galerkin and Galerkin least squares (GLS) methods show improved accuracy and a reduction in pollution error.

DEDICATION

This thesis is dedicated to my parents, whose loving support and constant encouragement are treasured forever.

ACKNOWLEDGEMENTS

I would like to express my sincere gratitude to my advisor, Professor Lonny L. Thompson, for sharing his knowledge, and providing invaluable guidance and constant support throughout the course of this work.

I would like to thank Professor Paul F. Joseph and Professor Sherrill B. Biggers for their help and for being a part of my thesis committee.

Special thanks are due to my parents, Dr. Subrahmanyam. C, and Subbalakshmi. C, and my brother Ramu for their encouragement, love, and support. I would also like to thank all my friends who made my stay at Clemson exciting, and memorable.

Finally, I would like to thank my fiancée, Lavanya, for her friendship, love, and support.

TABLE OF CONTENTS

	Page
TITLE PAGE	i
ABSTRACT	ii
DEDICATION	iii
ACKNOWLEDGEMENTS	iv
LIST OF TABLES	vii
LIST OF FIGURES	viii
 CHAPTER	
1. INTRODUCTION	1
Background	1
Objectives	5
2. TWO-DIMENSIONAL SPECTRAL ELEMENTS	7
Overview	7
Helmholtz Equation	7
Galerkin Finite Element Formulation	8
Dispersion Relationship	13
Selection of Quadrature Parameters	16
3. TWO-DIMENSIONAL NUMERICAL STUDIES	20
Overview	20
Model Problem	20
Numerical Results	40
4. HIGH-ORDER SPECTRAL ELEMENTS	51
Overview	51
Design of High-Order Spectral Element	51
Finite Element Formulation for Bi-Quadratic Interpolation	58

Table of Contents (Continued)

	Page
Galerkin Least Squares Formulation	61
Numerical Results	62
5. THREE-DIMENSIONAL SPECTRAL ELEMENTS.....	68
Overview	68
Galerkin Finite Element Formulation	68
Dispersion Relationship	71
Selection of Quadrature Parameters.....	73
Three-Dimensional Model Problem	76
Preliminary Results.....	86
6. CONCLUSIONS AND FUTURE WORK	88
Conclusions.....	88
Future Work	89
REFERENCES	91

LIST OF TABLES

Table	Page
2.1 Taylor series expansion of dispersion error	17
3.1 Quadrature rules on stiffness and mass matrices	30
5.1 3-D Quadrature parameters and corresponding methods.....	75

LIST OF FIGURES

Figure	Page
2.1 2-D bi-linear finite element mesh	15
2.2 Direction of plane-wave angle θ , measured relative to mesh lines	15
2.3 Normalized leading error vs. the wave angle θ	19
2.4 Normalized leading error vs. the wave angle θ	19
3.1 2-D Model problem.....	24
3.2 2-D Bi-linear square mesh	24
3.3 Stencil for edge nodes	39
3.4 Stencil for corner nodes	39
3.5 Real(ϕ) along the bottom edge, for $k = 30$, $kh = .75$, $\theta = 45$	44
3.6 Error measured in H_1 seminorm vs angle in degrees, for $k = 30$, $kh = .75$	44
3.7 Error measured in H_1 seminorm vs angle in degrees, for $k = 30$, $kh = .75$	45
3.8 Error measured in H_1 seminorm vs angle in degrees, for $k = 30$, $kh = 1.25$	45
3.9 Error measured in H_1 seminorm vs angle in degrees, for $k = 30$, $kh = 1.25$	46
3.10 Comparison of error for Galerkin and Spectral methods, $k = 30$	46
3.11 Convergence rates measured in H_1 seminorm	47
3.12 Pollution effect for $kh = 1.25$	47
3.13 Pollution error for increasing wavenumber at $\theta = 45$ and $kh = 1.25$	48
3.14 Error measured in L_2 norm vs angle in degrees, for $k = 30$, $kh = .75$	48

List of Figures (Continued)

Figure	Page
3.15 Error measured in L_2 norm vs angle in degrees, for $k = 30$, $kh = .75$	49
3.16 Pollution effect for $kh = .75$, error measured in L_2 norm	49
3.17 Convergence rates measured in L_2 norm	50
4.1 1-D quadratic mesh	55
4.2 Stencil for 1-D quadratic mesh	55
4.3 $\text{Real}(\phi)$ along the bottom edge, for $k = 30$, $kh = 1.5$, $\theta = 45$	64
4.4 Error measured in H_1 seminorm vs angle in degrees, for $k = 30$, $kh = 1.5$	64
4.5 Error measured in H_1 seminorm vs angle in degrees, for $k = 30$, $kh = 1.5$	65
4.6 $\text{Real}(\phi)$ along the bottom edge, for $k = 30$, $kh = 2$, $\theta = 45$	65
4.7 Error measured in H_1 seminorm vs angle in degrees, for $k = 30$, $kh = 2$	66
4.8 Error measured in H_1 seminorm vs angle in degrees, for $k = 30$, $kh = 2$	66
4.9 Convergence rates measured in H_1 seminorm	67
4.10 Pollution effect for $kh = 2$	67
5.1 3-D Model problem	81
5.2 Tri-linear finite element mesh	81
5.3 $\text{Real}(\phi)$ along the bottom edge, for $k = 30$, $kh = 1.5$, $\theta = 45$, $\phi = 0$	87

CHAPTER 1

INTRODUCTION

1.1 Background

This work deals with the development of accurate numerical methods for wave propagation problems. Wave propagation models a variety of physical phenomenon including acoustic, elastodynamic and electro-magnetic waves. Only a relatively few simple cases can be solved analytically, while a majority of practical problems must be solved by standard computational methods such as boundary element, finite difference and finite element methods.

A large class of wave propagation problems are governed by the scalar wave equation. For example, for sound waves propagating in a two-dimensional homogeneous, isotropic acoustic medium with wave speed c , the acoustic pressure $p(\mathbf{x}, t)$ satisfies,

$$\nabla^2 p(\mathbf{x}, t) - \frac{1}{c^2} \frac{\partial^2 p(\mathbf{x}, t)}{\partial t^2} = g(\mathbf{x}, t) \quad (1.1)$$

where $\mathbf{x} = (x, y)$ is the position vector in the solution domain Ω and t , denotes time in the interval $0 \leq t \leq T$. $\nabla^2 = \text{Div}(\text{Grad})$ is the Laplacian differential operator and g is an applied source function. For a time-harmonic source $g(\mathbf{x}, t) = f(\mathbf{x})e^{-i\omega t}$ driven at a frequency $\omega > 0$, solutions to equation 1.1 take the form $p(\mathbf{x}, t) = \phi(\mathbf{x})e^{-i\omega t}$ and satisfy the scalar Helmholtz (reduced wave) equation,

$$\nabla^2 \phi(\mathbf{x}) + k^2 \phi(\mathbf{x}) = -f(\mathbf{x}) \text{ in } \Omega \quad (1.2)$$

where $k = \omega / c > 0$, is the wave number with wavelength $\lambda = 2\pi / k$, and Ω is the spatial domain of interest. The Helmholtz equation in two-dimensions admits the plane wave propagating solution,

$$\phi(x, y) = e^{i(k_1 x + k_2 y)} \quad (1.3)$$

where k_1 and k_2 are the directional wave vector components given by $k_1 = k \cos\theta$, $k_2 = k \sin\theta$, θ is the plane wave orientation, and $k = \sqrt{k_1^2 + k_2^2}$.

Finite element solutions to the wave equation have primarily been sought using the standard Galerkin method, e.g., Maccamy and Marin [1980], Goldstein [1982], Bayliss, Goldstein and Turkel [1985] and Burnett [1993]. However, it is well known that the numerical phase accuracy of the standard Galerkin finite element solution deteriorates rapidly as the wave number, normalized with the element mesh size, is increased, Belytschko and Mullen [1978], Mullen and Belytschko [1982]. This resolution problem arises from the use of piecewise polynomial shape functions to approximate highly oscillatory wave propagation solutions. To obtain an acceptable level of accuracy, more than ten elements per wavelength are required and for large wave numbers, refining the mesh to maintain this requirement may become prohibitively expensive.

The propagation of waves in homogeneous, isotropic acoustic media is non-dispersive i.e. the wave number is linearly proportional to the frequency, $k = \omega / c$. The basic error of spatial discretization may be characterized as spurious dispersion since the wave number with which the approximate solution propagates depends on the resolution of the finite element mesh and is a non-linear function of frequency. Dispersion analysis relates the normalized frequency $k = \omega / c$ with the finite element discrete wave number

k^h . This relationship is called the characteristic equation. Recent studies, Babuska, et.al. [1995], show that the error of the finite element solution in the frequency domain is small if the wave number $k = \omega / c$ normalized with the element size h , given by kh is small. However, for large k , and fixed kh , the dispersion error increases due to pollution effect as a result of boundary conditions.

Several approaches to improve the accuracy of the standard Galerkin method for solutions to the Helmholtz equation have been proposed in recent years. Babuska et.al. [1995] proposed the Generalized Finite Element Method (GFEM) in which local mappings are introduced which transform the usual finite element basis functions to another local basis. These local mappings are designed in such a way that the resulting method applied to a differential equation converges with an optimal rate. However, the optimal rate is valid only for uniform square meshes.

In the recent years, a new class of residual based finite element formulations has emerged to improve the stability and hence accuracy of the standard Galerkin method for the Helmholtz equation. These methods are developed by appending residuals of the Helmholtz equation in least-squares form to the standard Galerkin variational equation, hence the name Galerkin least squares (GLS) method. The GLS method employs a mesh parameter that is designed to minimize dispersion error appearing in the characteristic equation, allowing the use of a reduced number of elements per wavelength. The added terms preserve the consistency inherent in the parent Galerkin method. Harari and Hughes [1992], have developed GLS methods for the Helmholtz equation in one-dimension and applied this to multi-dimensional problems Harari [1991]. Thompson and Pinsky [1995]

developed an improved GLS mesh parameter for multi-dimensions and derived an optimal parameter for higher-order accurate quadratic elements.

Both the GFEM and GLS methods decrease the number of elements required to achieve a desired level of accuracy at any given frequency, thereby allowing for the solution of large scale structural acoustics problems at higher frequencies. However, in these methods the element matrices are dependent on the wave frequency ω , and hence cannot be used directly for transient wave propagation. For the Galerkin method, the assembled matrix equations for the Helmholtz problem, equation 1.2, take the form,

$$(\mathbf{K} - k^2 \mathbf{M}) \mathbf{d} = \mathbf{F} \quad (1.4)$$

where \mathbf{K} and \mathbf{M} are frequency independent stiffness and mass arrays respectively and \mathbf{d} is the global solution vector. Direct application of the inverse Fourier transform results in the time-dependent discretization of the wave equation 1.1,

$$\mathbf{K}\mathbf{P}(t) + \frac{1}{c^2} \mathbf{M} \frac{\partial^2 \mathbf{P}(t)}{\partial t^2} = \mathbf{Q}(t) \quad (1.5)$$

Since \mathbf{K} and \mathbf{M} are independent of frequency they can be used directly for solutions to the time harmonic equation 1.4 or the time dependent equation 1.5.

For the GLS method with linear elements the matrix equations resulting from the discretization of the Helmholtz equation 1.2 take the form,

$$(\mathbf{K} - k^2 \mathbf{M}_{GLS}) \mathbf{d} = \mathbf{F}_{GLS} \quad (1.6)$$

where

$$\mathbf{M}_{GLS} = (1 - \tau k^2) \mathbf{M} , \quad (1.7)$$

with frequency (wavenumber) dependent mesh parameter $\tau(k)$. For reduced dispersion error τ is a highly nonlinear function in k , and as a result, direct use of an inverse Fourier transform is not possible, hence this method cannot be used directly to solve the scalar wave equation in the time-domain. A similar limitation is present in the GFEM method with matrix equations taking the form,

$$\mathbf{A}(k)\mathbf{d} = \mathbf{F}. \quad (1.8)$$

As a result of the frequency dependent coefficient matrix \mathbf{A} , the method cannot be used directly in the time-domain.

1.2 Objectives

The objective of this work is to develop a high-order accurate Spectral element method based on optimal quadrature rules which reduce dispersion error and which can be used directly in both the frequency and time domains. To study the accuracy compared to various modified Galerkin methods, we consider the numerical solution to the two-dimensional Helmholtz equation defined on a bi-unit square domain. Non-reflecting boundary conditions are specified on the four edges of the computational domain which allow for plane wave solutions propagating at different orientations with respect to horizontal and vertical mesh lines. The non-reflecting boundary condition takes the form of a linear relation between the solution and its normal derivative on the boundary.

Specific Aims

1. Using a two-dimensional dispersion analysis of the Galerkin finite element method using bi-linear shape functions, determine optimal quadrature rules which reduce dispersion.

2. Compare dispersion relations for different quadrature rules corresponding to standard and modified Galerkin methods as a function of the number of elements per wavelength (normalized wavenumber kh) and plane-wave orientation.
3. Verify the accuracy of optimal quadrature rules compared to competing methods based on numerical solution of two-dimensional plane-wave model problem and study pollution effect for high wavenumbers. Measure error based on L_2 norm and H_1 semi norm as a function of plane-wave orientation angle θ .
4. Using a one-dimensional dispersion analysis, derive optimal quadrature rules for elements based on quadratic shape functions. Compare dispersion relations as a function of kh .
5. Compare accuracy of biquadratic Spectral elements based on optimal quadrature rules in one-dimension with GLS methods for the two-dimensional plane-wave model problem.
6. Using a three-dimension dispersion analysis, derive optimal quadrature rules for tri-linear elements.
7. Extend two-dimensional model problem to three-dimensions and compare the accuracy of tri-linear spectral element with Standard Galerkin finite element method.

CHAPTER 2

TWO-DIMENSIONAL SPECTRAL ELEMENTS

2.1 Overview

In this chapter, optimal quadrature rules are determined for four-node elements with bi-linear shape functions which reduce dispersion error and minimize the pollution effect for wave propagation in two-dimensions. The quadrature rules are obtained from a Taylor series expansion of the characteristic equation relating the normalized frequency $k = \omega / c$, and the wave vector components k_1^h and k_2^h from a two-dimensional mesh of bi-linear elements. Optimal quadrature rules are identified which annihilate the leading dispersion error terms in this expansion, resulting in a high-order accurate spectral element. Other modified Galerkin finite elements and their associated quadrature points are compared, including consistent, lumped, and high-order mass arrays.

2.2 Helmholtz Equation

Consider the two-dimensional Helmholtz equation:

$$\nabla^2 \phi(x, y) + k^2 \phi(x, y) = -f \quad \text{in } \Omega \quad (2.1)$$

where, $k = \omega / c > 0$, is the normalized frequency, ∇^2 is the Laplacian differential operator and Ω is the spatial domain of interest. As discussed earlier, equation 2.1 admits the plane-wave solution,

$$\phi(x, y) = Ae^{i(k_1 x + k_2 y)} \quad (2.2)$$

with wave vector components,

$$\begin{aligned} k_1 &= k \cos \theta \\ k_2 &= k \sin \theta \end{aligned} \quad (2.3)$$

such that $k^2 = k_1^2 + k_2^2$ and θ is the wave angle relative to the x-axis.

2.3 Galerkin Finite Element Formulation

Consider the partition of Ω into finite elements. Let Ω^e be the interior of the e^{th} element, and $\Omega^h = \bigcup_{e=1}^N \Omega_e$ where N is the number of elements in the mesh. The standard

Galerkin finite element variational equation corresponding to equation 2.1 is,

$$A(w^h, \phi^h) = L(w^h) \quad (2.4)$$

where

$$A(w^h, \phi^h) = \int_{\Omega} \nabla w^h \bullet \nabla \phi^h d\Omega - k^2 \int_{\Omega} w^h \phi^h d\Omega \quad (2.5)$$

$$L(w^h) = \int_{\Omega} w^h f d\Omega \quad (2.6)$$

where w^h is the approximate trial (weighting) function and $\phi^h \approx \phi$ is the approximate solution.

For dispersion analysis, we consider an infinite domain Ω and neglect boundary conditions. The domain Ω is discretized by a uniform mesh of bi-linear square elements, with edge width h . The element domain is parameterized over the bi-unit square $-1 \leq \xi \leq 1$, $-1 \leq \eta \leq 1$, with the usual mapping,

$$\mathbf{x}(\xi, \eta) = \sum_{i=1}^4 N_i^e(\xi, \eta) \mathbf{x}_i^e, \quad \mathbf{x} \in \Omega_e \quad (2.7)$$

where $x_i^e = \mathbf{x}(\xi, \eta)$ are nodal coordinates and N_i^e are bi-linear shape functions defined as,

$$N_i^e(\xi, \eta) = \frac{1}{4}(1 + \xi_i \xi)(1 + \eta_i \eta) \quad (2.8)$$

For a square element the Jacobian simplifies to

$$J^e = \det(\mathbf{x}/\underline{\xi}) = h^2 / 4 \quad (2.9)$$

where

$$\mathbf{x} = \begin{bmatrix} x \\ y \end{bmatrix}, \quad \underline{\xi} = \begin{bmatrix} \xi \\ \eta \end{bmatrix} \quad (2.10)$$

The finite element approximation within each element defined in terms of the nodal degrees of freedom (dof),

$$\phi^h(\xi, \eta) = \sum_{i=1}^4 N_i^e(\xi, \eta) \phi_i^e, \quad (\xi, \eta) \in (-1, 1)^2 \quad (2.11)$$

and associated weighting function,

$$w^h(\xi, \eta) = \sum_{i=1}^4 N_i^e(\xi, \eta) w_i^e, \quad (\xi, \eta) \in (-1, 1)^2 \quad (2.12)$$

where, $\phi_i^e = \phi^h(\xi_i, \eta_i)$ and $w_i^e = w^h(\xi_i, \eta_i)$ are the element nodal dof and nodal weighting parameters respectively. For dispersion analysis we assume a uniform infinite mesh with homogeneous source $f = 0$. Substituting equations 2.11 and 2.12 into equation 2.4 leads to the (4x4) element dynamic matrix \mathbf{s}^e composed of the stiffness and mass arrays.

$$\mathbf{s}^e = \mathbf{k}^e - k^2 \mathbf{m}^e \quad (2.13)$$

where,

$$\mathbf{k}^e = [k_{ij}^e] \quad (2.14)$$

$$\mathbf{m}^e = [m_{ij}^e]. \quad (2.15)$$

The stiffness coefficients are,

$$\begin{aligned} k_{ij}^e &= \int_{\Omega^e} \left(\frac{\partial N_i}{\partial x} \frac{\partial N_j}{\partial x} + \frac{\partial N_i}{\partial y} \frac{\partial N_j}{\partial y} \right) d\Omega \\ &= \int_{-1}^1 \int_{-1}^1 \left(\frac{\partial N_i}{\partial \xi} \frac{\partial N_j}{\partial \xi} + \frac{\partial N_i}{\partial \eta} \frac{\partial N_j}{\partial \eta} \right) \frac{1}{J^e} d\xi d\eta \end{aligned} \quad (2.16)$$

and the mass coefficients are,

$$m_{ij}^e = \int_{\Omega^e} N_i N_j d\Omega = \int_{-1}^1 \int_{-1}^1 N_i N_j J^e d\xi d\eta. \quad (2.17)$$

The integrals over the bi-unit square are evaluated using numerical quadrature,

$$\begin{aligned} k_{ij}^e &= \frac{4}{h^2} \sum_{p=1}^{n_p} \sum_{q=1}^{n_q} \left\{ \frac{\partial N_i(\xi_p, \eta_q)}{\partial \xi} \frac{\partial N_j(\xi_p, \eta_q)}{\partial \xi} \right. \\ &\quad \left. + \frac{\partial N_i(\xi_p, \eta_q)}{\partial \eta} \frac{\partial N_j(\xi_p, \eta_q)}{\partial \eta} \right\} \times w_p \times w_q \end{aligned} \quad (2.18)$$

and

$$m_{ij}^e = \frac{h^2}{4} \sum_{a=1}^{n_a} \sum_{b=1}^{n_b} N_i(\xi_a, \eta_b) N_j(\xi_a, \eta_b) w_a \times w_b. \quad (2.19)$$

In the following we assume symmetric quadrature rules and the number of quadrature points in each direction $n_p = n_q = 2$ and $n_a = n_b = 2$. Independent quadrature points are defined for evaluation of stiffness and mass coefficients. In order to satisfy the condition that quadrature should exactly integrate constants, ($w_1 + w_2 = 2$), then for symmetric weights, $w_1 = w_2 = 1$.

For the stiffness matrix,

$$\begin{aligned}\xi_1 &= -\xi_2 = x_k \\ \eta_1 &= -\eta_2 = x_k.\end{aligned}\tag{2.20}$$

For the mass matrix,

$$\begin{aligned}\xi_1 &= -\xi_2 = x_m \\ \eta_1 &= -\eta_2 = x_m.\end{aligned}\tag{2.21}$$

For Gauss quadrature, $x_k = x_m = 1/\sqrt{3}$, for Lobatto quadrature (Trapezoidal rule) the quadrature points are taken at the nodes, $x_k = x_m = 1$. Based on these assumptions on quadrature rules, the symmetric stiffness and mass matrices take the form,

$$\mathbf{k}^e = \begin{bmatrix} a_1 & a_2 & a_3 & a_2 \\ & a_1 & a_2 & a_3 \\ sym & a_1 & a_2 & \\ & & a_1 & \end{bmatrix}, \quad \mathbf{m}^e = \begin{bmatrix} b_1 & b_2 & b_3 & b_2 \\ & b_1 & b_2 & b_3 \\ sym & b_1 & b_2 & \\ & & b_1 & \end{bmatrix}.\tag{2.22}$$

Due to symmetry, there are only three independent stiffness coefficients,

$$\begin{aligned}a_1 &= \frac{1}{2}(1 + x_k^2), \\ a_2 &= -\frac{1}{2}x_k^2, \\ a_3 &= \frac{1}{2}(x_k^2 - 1).\end{aligned}\tag{2.23}$$

Similarly, there are three independent mass coefficients,

$$\begin{aligned}b_1 &= \beta(1 + x_m^2)^2, \\ b_2 &= \beta(1 - x_m^4), \\ b_3 &= \beta(1 - x_m^2)^2,\end{aligned}\tag{2.24}$$

where $\beta = h^2 / 16$. The difference stencil associated with a typical interior node $\phi^h(x_m, y_n) = \phi_{m,n}$ is obtained by assembling element arrays for a patch of four connecting elements as illustrated in Figure 2.1. The resulting stencil may be written as,

$$(S - k^2 M)\phi_{m,n} = 0 \quad (2.25)$$

where S and M are the two-dimensional linear difference operators emanating from the assembled stiffness and mass matrices respectively.

$$S = S_x + S_y \quad (2.26)$$

where

$$S_x = -\frac{1}{h^2} \left(1 + \frac{\epsilon_k}{6} \delta_y^2\right) \delta_x^2 \quad (2.27)$$

$$S_y = -\frac{1}{h^2} \left(1 + \frac{\epsilon_k}{6} \delta_x^2\right) \delta_y^2 \quad (2.28)$$

and

$$M = M_x M_y \quad (2.29)$$

where

$$M_x = \left(1 + \frac{\epsilon_m}{6} \delta_x^2\right) \quad (2.30)$$

$$M_y = \left(1 + \frac{\epsilon_m}{6} \delta_y^2\right). \quad (2.31)$$

The central difference operators are defined by,

$$\delta_x^2 \phi_{m,n} = \phi_{m-1,n} - 2\phi_{m,n} + \phi_{m+1,n}, \quad (2.32)$$

$$\delta_y^2 \phi_{m,n} = \phi_{m,n-1} - 2\phi_{m,n} + \phi_{m,n+1}. \quad (2.33)$$

$0 \leq \varepsilon_k \leq 1, 0 \leq \varepsilon_m \leq 1$ are parameterized quadrature points defined as,

$$\varepsilon_k = \frac{3}{2}(1 - x_k^2) \text{ and } \varepsilon_m = \frac{3}{2}(1 - x_m^2). \quad (2.34)$$

Gauss quadrature corresponds to $\varepsilon_k = \varepsilon_m = 1$, while Lobatto corresponds to $\varepsilon_k = \varepsilon_m = 0$.

2.4 Dispersion Relationship

The characteristic equation relating the normalized frequency k with the numerical wavenumber vector components $k_1^h = k^h \cos\theta$ and $k_2^h = k^h \sin\theta$ is obtained by assuming a nodal solution which takes the form of the analytical solution, i.e., a plane wave solution oriented at an angle θ with respect to horizontal mesh lines, see Figure 2.2. The assumed solution at a typical node is,

$$\phi_{m,n} = A^h e^{i(k_1^h h m + k_2^h h n)}. \quad (2.35)$$

Substituting equation 2.35 into 2.25 leads to the dispersion relation,

$$\tilde{S} - k^2 \tilde{M} = 0. \quad (2.36)$$

In this relation, \tilde{S} and \tilde{M} represent the wavenumber dependent stiffness and mass operators respectively, and are defined as,

$$\tilde{S} = \mathbf{1}_y^k \bar{k}_x^2 + \mathbf{1}_x^k \bar{k}_y^2 \quad (2.37)$$

$$\tilde{M} = \mathbf{1}_x^m \mathbf{1}_y^m \quad (2.38)$$

with notation,

$$\bar{k}_x^2 = \frac{2}{h^2}(1 - C_x) \text{ and } \bar{k}_y^2 = \frac{2}{h^2}(1 - C_y) \quad (2.39)$$

$$C_x = \cos(k_1^h h) = \cos(k^h h \cos\theta) \quad (2.40)$$

$$C_y = \cos(k_2^h h) = \cos(k^h h \sin \theta) \quad (2.41)$$

$$1_x^k = 1 - \frac{\epsilon_k}{6} (\bar{k}_x h)^2 \quad (2.42)$$

$$1_y^k = 1 - \frac{\epsilon_k}{6} (\bar{k}_y h)^2 \quad (2.43)$$

$$1_x^m = 1 - \frac{\epsilon_m}{6} (\bar{k}_x h)^2 \quad (2.44)$$

$$1_y^m = 1 - \frac{\epsilon_m}{6} (\bar{k}_y h)^2. \quad (2.45)$$

Rearranging,

$$k^2 = \frac{\tilde{S}}{\tilde{M}} = \frac{1_y^k \bar{k}_x^2 + 1_x^k \bar{k}_y^2}{1_x^m 1_y^m}. \quad (2.46)$$

It is clear that the dispersion relation depends on both the magnitude of the discrete wave number k^h and the orientation of the wave vector θ given by,

$$(k^h)^2 = (k_1^h)^2 + (k_2^h)^2 \quad (2.47)$$

$$\theta = \arctan(k_2^h / k_1^h). \quad (2.48)$$

The exact relation is,

$$k^2 = k_1^2 + k_2^2. \quad (2.49)$$

In the limit $k^h h \rightarrow 0$, corresponding to a large number of elements per wavelength, the discrete dispersion relation, equation 2.46, converges to the exact relation, equation 2.49, for any choice of quadrature point. However, for finite values of $k^h h$, the dispersion error in the finite element approximation is,

$$E_k = k^2 - (k^h)^2 = \frac{\tilde{S}}{\tilde{M}} - (k^h)^2. \quad (2.50)$$

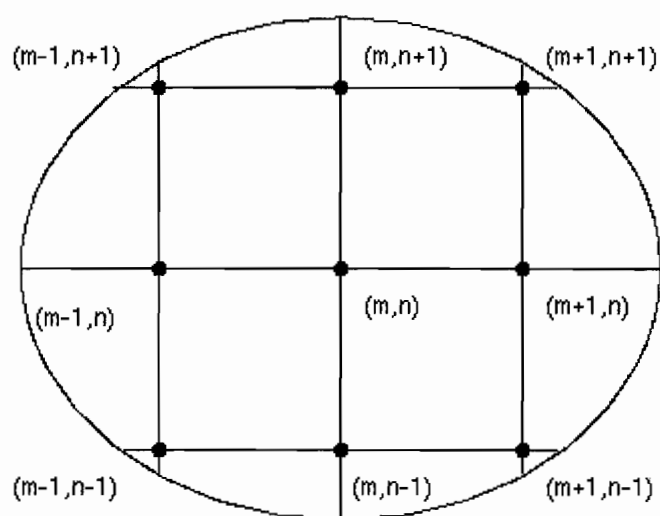


Figure 2.1 2-D bi-linear finite element mesh.

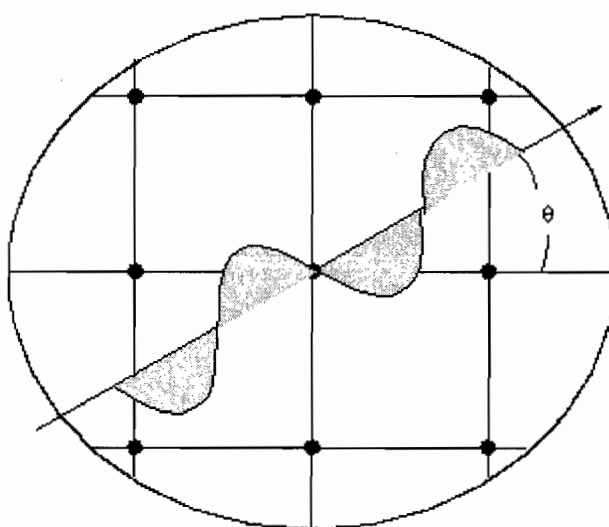


Figure 2.2 Direction of plane-wave angle θ , measured relative to mesh lines.

2.4 Selection of Quadrature Points

In this section optimal values are determined for the parameterized quadrature points ϵ_k and ϵ_m which reduce dispersion error. Expanding the dispersion relation, equation 2.46 in a multi-Taylor's series expansion of k_1^h and k_2^h yields,

$$\begin{aligned} k^2 = (k^h)^2 &+ \left[\left(-\frac{1}{12}\right)h^2 + \left(\frac{1}{6}\right)h^2 \epsilon_m \right] (k_1^h)^4 + \\ &\left[\left(-\frac{1}{3}\right)\epsilon_k h^2 + \left(\frac{1}{3}\right)\epsilon_m h^2 \right] (k_1^h)^2 (k_2^h)^2 + \\ &\left[\left(-\frac{1}{12}\right)h^2 + \left(\frac{1}{6}\right)h^2 \epsilon_m \right] (k_2^h)^4 + \dots \end{aligned} \quad (2.51)$$

From equation 2.51, the leading error term is annihilated by the quadrature points,

$$\epsilon = \epsilon_k = \epsilon_m = 1/2 \quad (2.52)$$

corresponding to $x_k = x_m = \sqrt{2/3}$, leaving an error of sixth-order only. The quadrature rules with the above conditions are,

$$\begin{aligned} \xi_1 &= -\xi_2 = \sqrt{2/3} \\ \eta_1 &= -\eta_2 = \sqrt{2/3} \\ w_1 &= w_2 = 1 \end{aligned} \quad (2.53)$$

on both the stiffness and the mass terms defines the high-order accurate four-node bilinear Spectral element. For comparison, the leading dispersion error resulting from a Taylor series expansion is given in Table 2.1 for several values of quadrature points.

Table 2.1
Taylor Series Expansion of Dispersion Error

Method	ϵ_k	ϵ_m	$E_k = k^2 - (k^h)^2$
Finite Difference	0	0	$-\frac{h^2}{12}((k_1^h)^4 + (k_2^h)^4)$
Galerkin, Consistent Mass	1	1	$\frac{h^2}{12}((k_1^h)^4 + (k_2^h)^4)$
Galerkin, Diagonal Mass	1	0	$-\frac{h^2}{12}((k_1^h)^4 + (k_2^h)^4) + \frac{h^2}{4}((k_1^h)^2 (k_2^h)^2)$
Galerkin, High-Order Mass	1	$\frac{1}{2}$	$-\frac{h^2}{6}((k_1^h)^2 (k_2^h)^2)$
Spectral	$\frac{1}{2}$	$\frac{1}{2}$	$-\frac{h^2}{240}((k_1^h)^6 + (k_2^h)^6)$
Spectral, Diagonal Mass	$\frac{1}{2}$	0	$-\frac{h^2}{12}(k^h)^4$

From the above table it can be seen that the spectral elements result in a smaller error than the alternative methods. When using an explicit time-integration of the semi-discrete equations, equation 2.1, a diagonal mass matrix is required. In this case the spectral element with diagonal mass corresponding to quadrature points $x_k = \sqrt{2/3}$ and $x_m = 1$, is optimal in that the leading error term is isotropic, i.e., E_k is independent of the wave

orientation angle θ . The normalized leading error term in Taylor series expansion of dispersion relation for fourth order accurate methods is defined as,

$$E_N = \frac{E_k}{(k^h)^4 h^2} \quad (2.54)$$

and for sixth order accurate spectral method,

$$E_N = \frac{E_k}{(k^h)^6 h^2}. \quad (2.55)$$

The magnitude of the normalized leading error term as a function of the wave angle θ , for various methods is plotted in Figures 2.3 and 2.4. The dispersion error for the spectral element is,

$$E_k = \frac{\left(\frac{1}{h^2}\right)\left(\frac{10}{3} - 3c_x - 3c_y + c_x c_y\right)}{\left(1 - \frac{1}{6}(1 - c_x)\right)\left(1 - \frac{1}{6}(1 - c_y)\right)} \quad (2.56)$$

and for the Spectral element with diagonal mass,

$$E_k = \frac{2}{3h^2}(7 - 4c_x - 4c_y + c_x c_y). \quad (2.57)$$

Remark:

The use of Gauss quadrature points $x_k = \sqrt{1/3}$ for stiffness and spectral quadrature points $x_m = \sqrt{2/3}$ for mass is denoted as high-order mass and gives high-order accuracy as the spectral element for waves propagating along the mesh lines, i.e., $k_1^h = 0$ at $\theta = 0$, or $k_2^h = 0$ at $\theta = \pi/2$, resulting in E_k of order 6.

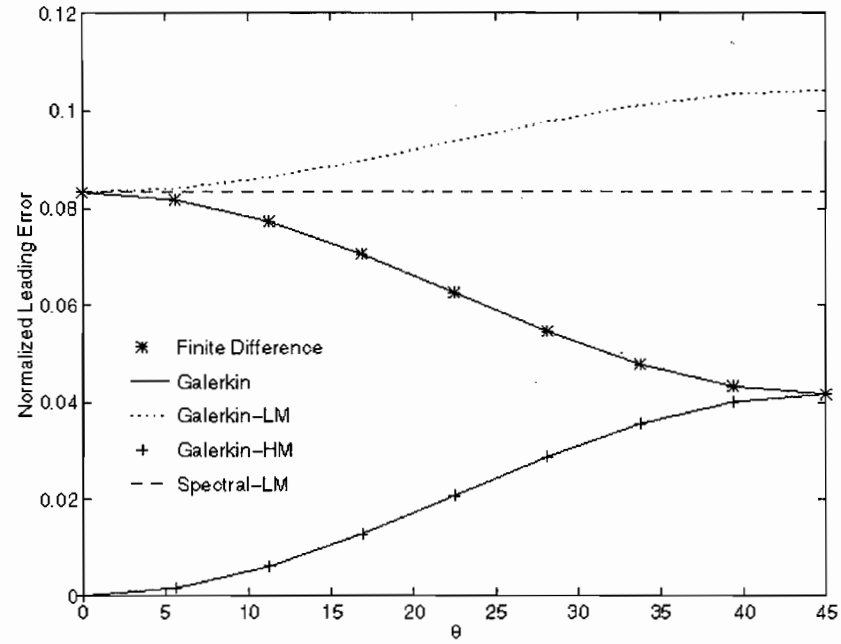


Figure 2.3 Normalized leading error term vs wave angle θ .

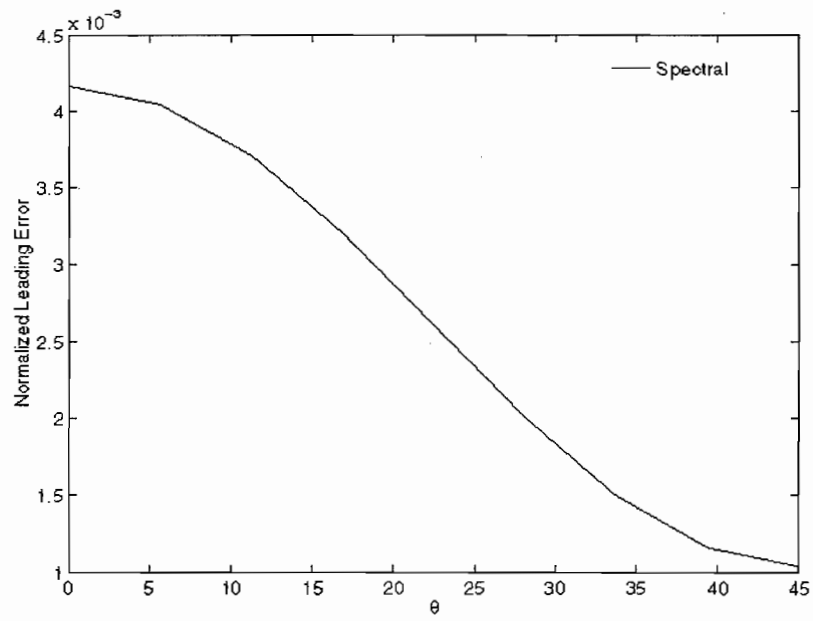


Figure 2.4 Normalized leading error term vs wave angle θ .

CHAPTER 3

2-D NUMERICAL STUDIES

3.1 Overview

In this chapter the accuracy of the spectral element for a model problem including non-reflecting boundaries is studied. The non-reflecting boundary conditions on the edges of the computational domain are designed to allow propagating plane wave solutions at different orientations.

3.2 Model Problem

3.2.1 Strong form of the Boundary Value Problem (BVP)

Consider a BVP for plane wave propagation on a bi-unit square domain, see Figure 3.1. The objective is to find $\phi(x,y)$, the spatial component of the acoustic pressure such that the Helmholtz equation is satisfied:

$$\nabla^2 \phi + k^2 \phi = 0 \quad \text{in } \Omega := (0,1) \times (0,1) \quad (3.1)$$

with non-reflecting boundary conditions on all four edges,

$$ik\phi + \frac{\partial \phi}{\partial n} = g \quad \text{on } \Gamma_s \text{ for } s \in \{1,2,3,4\}. \quad (3.2)$$

In the above, $k = \omega / c$ is the wave number, $i = \sqrt{-1}$, $\partial / \partial n$ is the normal derivative on Γ_s .

The function g depends on k and θ :

$$\begin{aligned}
 g(\mathbf{x}) &= g_1(x) && \text{for } \mathbf{x} \in \Gamma_1 := (0,1) \times (0,0) \\
 &= g_2(y) && \text{for } \mathbf{x} \in \Gamma_2 := (1,1) \times (0,1) \\
 &= g_3(x) && \text{for } \mathbf{x} \in \Gamma_3 := (0,1) \times (1,1) \\
 &= g_4(y) && \text{for } \mathbf{x} \in \Gamma_4 := (0,0) \times (0,1)
 \end{aligned} \tag{3.3}$$

where

$$\begin{aligned}
 g_1(x) &= i(k - k_2)e^{ik_1x} \\
 g_2(y) &= i(k + k_1)e^{i(k_1+k_2)y} \\
 g_3(x) &= i(k + k_2)e^{i(k_1x+k_2)} \\
 g_4(y) &= i(k - k_1)e^{ik_2y}
 \end{aligned} \tag{3.4}$$

and

$$k_1 = k \cos \theta, \quad k_2 = k \sin \theta \tag{3.5}$$

The boundary condition, equation 3.2, is designed so that the exact solution to the BVP is the plane-wave solution, $\phi(x, y) = e^{ik(x \cos \theta + y \sin \theta)}$.

3.2.2 Weak form of the BVP

The weak form of the BVP can be obtained formally by multiplying equation 3.1 with the complex conjugate of a weighting function. Then, after integration by parts and substitution of the natural boundary conditions, equation 3.2 and 3.3, we arrive at the variational problem: Find ϕ such that for all w ,

$$A(w, \phi) = L(w) \tag{3.6}$$

where,

$$A(w, \phi) = \int_{\Omega} \nabla w \bullet \nabla \phi \, d\Omega - k^2 \int_{\Omega} w \phi \, d\Omega + ik \int_{\Gamma} w \phi \, d\Gamma \tag{3.7}$$

and

$$L(w) = \int_{\Gamma} w g d\Gamma = \sum_{s=1}^4 \int_{\Gamma_s} w_s g_s d\Gamma \quad (3.8)$$

The bi-linear operator A, involves a complex number term on the boundary Γ due to the form of equation 3.2. The linear operator L, also is complex due to the definition of g.

3.2.3 Galerkin Form of the BVP

The Galerkin form of the BVP is simply a re-statement of the weak form with the solution function $\phi(x, y)$ replaced by an approximate solution $\phi^h(x, y)$, and the weighting function $w(x, y)$ replaced by an approximate weighting function $w^h(x, y)$, i.e.

$$\begin{aligned} \phi(x, y) &\approx \phi^h(x, y) \\ w(x, y) &\approx w^h(x, y) \end{aligned} \quad (3.9)$$

The superscript h is used to indicate that the quantity is an approximation. Making these substitutions the Galerkin form of the BVP can be defined as: Find $\phi^h(x, y)$, such that for all $w^h(x, y)$,

$$A(w^h, \phi^h) = L(w^h) \quad (3.10)$$

where

$$A(w^h, \phi^h) = \int_{\Omega} \nabla w^h \bullet \nabla \phi^h d\Omega - k^2 \int_{\Omega} w^h \phi^h d\Omega + ik \int_{\Gamma} w^h \phi^h d\Gamma \quad (3.11)$$

$$L(w^h) = \int_{\Gamma} w^h g d\Gamma \quad (3.12)$$

3.2.4 Finite Element Formulation

The finite element analysis of the above model problem was performed using a mesh of four-node bilinear square elements. The domain is discretized into n finite elements as shown in Figure 3.2. The elements are arbitrarily numbered from bottom left corner starting at 1 and running to n to the top right corner. Consider a typical element e , such that $1 \leq e \leq n$, and let the interval covered by the element e to be denoted by Ω^e such that,

$$\Omega = \Omega^1 \cup \Omega^2 \cup \dots \cup \Omega^e \cup \dots \cup \Omega^n. \quad (3.13)$$

After discretization, the integral over the domain Ω can be written as a sum of integrals over each element domain, i.e.,

$$\int_{\Omega} (\bullet) d\Omega = \sum_{e=1}^n \int_{\Omega^e} (\bullet) d\Omega^e \quad (3.14)$$

so that the Galerkin variational equation can be written as,

$$\begin{aligned} \sum_{e=1}^n \left[\int_{\Omega^e} \nabla w^h \bullet \nabla \phi^h d\Omega^e - k^2 \int_{\Omega^e} w^h \phi^h d\Omega^e + ik \int_{\Gamma^e} w^h \phi^h d\Gamma^e \right] \\ = \sum_{e=1}^n \int_{\Gamma^e} w^h g d\Gamma^e \end{aligned} \quad (3.15)$$

The finite element approximation within each element can be written as an interpolation of the nodal degrees of freedom,

$$\phi^h = \sum_{i=1}^l N_i^e d_i^e \quad (3.16)$$

where N_i^e is the shape function of the i^{th} node of element e and l is the number of degrees of freedom per element. For a four node element, $l = 4$. The approximation,

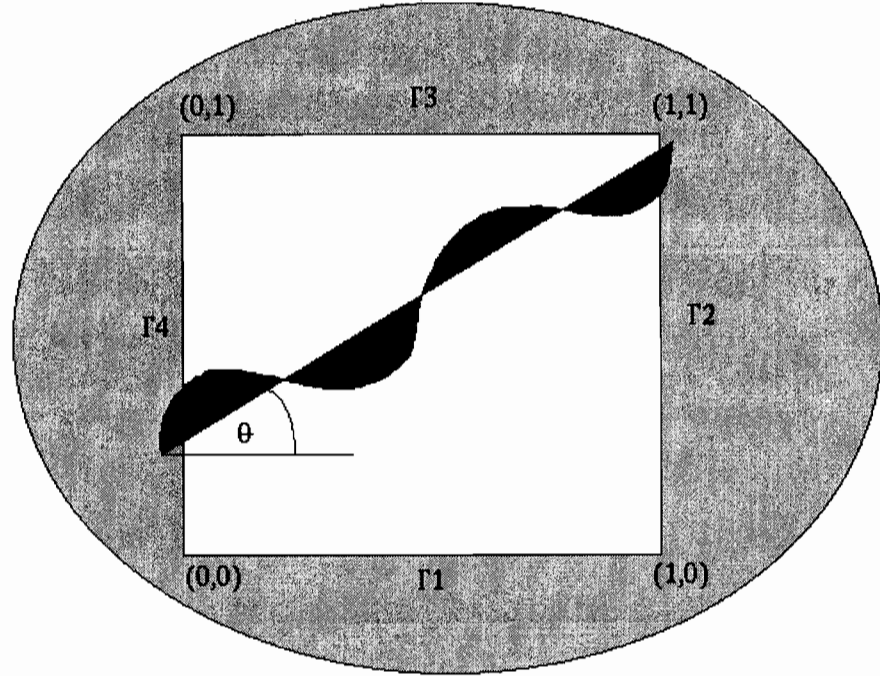


Figure 3.1 2-D Model Problem

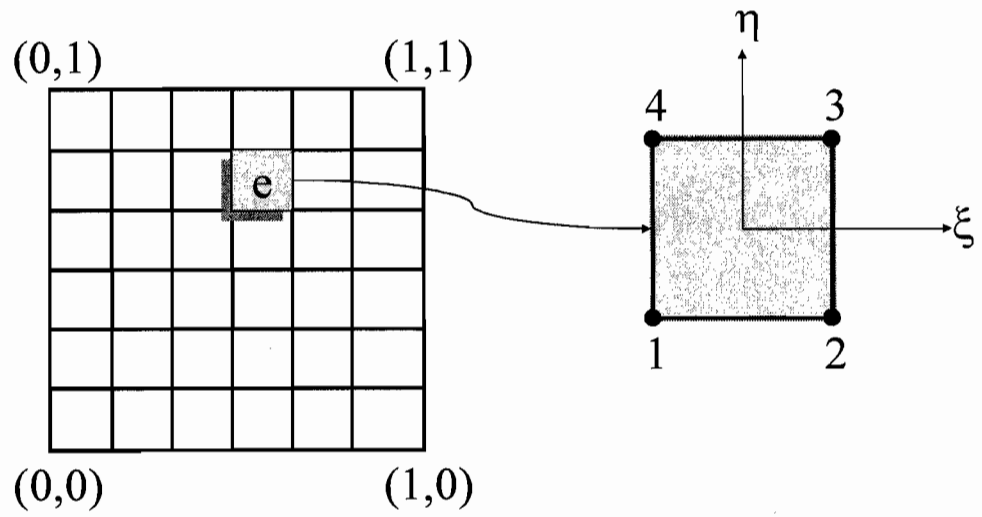


Figure 3.2 2-D Bi-linear square mesh

equation 3.16 can also be written in matrix form as,

$$\phi^h = \mathbf{N}^e \mathbf{d}^e \quad (3.17)$$

where,

$$\mathbf{N}^e = [N_1^e \ N_2^e \ N_3^e \ N_4^e] \quad (3.18)$$

is the shape function array, where the shape functions N_i^e are standard bi-linear Lagrange functions defined as,

$$\begin{aligned} N_1^e &= \frac{1}{4}(1-\xi)(1-\eta), \\ N_2^e &= \frac{1}{4}(1+\xi)(1-\eta), \\ N_3^e &= \frac{1}{4}(1+\xi)(1+\eta), \\ N_4^e &= \frac{1}{4}(1-\xi)(1+\eta). \end{aligned} \quad (3.19)$$

$$\mathbf{d}^e = [d_1^e \ d_2^e \ d_3^e \ d_4^e]^T \quad (3.20)$$

is the element degree of freedom vector. Similarly the weighting function can be written as,

$$w^h = \mathbf{N}^e \delta \mathbf{d}^e. \quad (3.21)$$

Using the above approximations, the gradient can be written as,

$$\nabla \phi^h = \begin{bmatrix} \frac{\partial \phi^h}{\partial x} \\ \frac{\partial \phi^h}{\partial y} \end{bmatrix} = \mathbf{B}^e \mathbf{d}^e \quad (3.22)$$

where

$$\mathbf{B}^e = \begin{bmatrix} N_{1,x}^e, N_{2,x}^e, N_{3,x}^e, N_{4,x}^e \\ N_{1,y}^e, N_{2,y}^e, N_{3,y}^e, N_{4,y}^e \end{bmatrix} \quad (3.23)$$

Similarly the gradient of the weighting function can be written as,

$$\nabla w^h = \mathbf{B}^e \delta \mathbf{d}^e. \quad (3.24)$$

Substituting the finite element approximation, equation 3.17 into equation 3.15 gives,

$$\begin{aligned} \sum_{e=1}^n \delta \mathbf{d}^{eT} \left\{ \int_{\Omega^e} \mathbf{B}^{eT} \mathbf{B}^e d\Omega^e - k^2 \int_{\Omega^e} \mathbf{N}^{eT} \mathbf{N}^e d\Omega^e + ik \int_{\Gamma^e} \mathbf{N}^{eT} \mathbf{N}^e d\Gamma^e \right\} \mathbf{d}^e \\ = \sum_{e=1}^n \delta \mathbf{d}^{eT} \int_{\Gamma^e} \mathbf{N}^{eT} g d\Gamma^e. \end{aligned} \quad (3.25)$$

Defining the element matrices,

$$\mathbf{k}^e = \int_{\Omega^e} \mathbf{B}^{eT} \mathbf{B}^e d\Omega^e \quad (\text{element stiffness matrix}) \quad (3.26)$$

$$\mathbf{m}^e = \int_{\Omega^e} \mathbf{N}^{eT} \mathbf{N}^e d\Omega^e \quad (\text{element mass matrix}) \quad (3.27)$$

$$\mathbf{b}^e = \int_{\Gamma^e} \mathbf{N}^{eT} \mathbf{N}^e d\Gamma^e \quad (\text{element boundary condition matrix}) \quad (3.28)$$

$$\mathbf{f}^e = \int_{\Gamma^e} \mathbf{N}^{eT} g d\Gamma^e \quad (\text{element load vector}). \quad (3.29)$$

Equation 3.25 may be written as,

$$\sum_{e=1}^n \delta \mathbf{d}^{eT} \left\{ \mathbf{k}^e - k^2 \mathbf{m}^e + ik \mathbf{b}^e \right\} \mathbf{d}^e = \sum_{e=1}^n \delta \mathbf{d}^{eT} \mathbf{f}^e. \quad (3.30)$$

Relating local dof \mathbf{d}^e to global dof \mathbf{d} and assembly leads to the global matrix problem,

$$(\mathbf{K} - k^2 \mathbf{M} + ik \mathbf{B}) \mathbf{d} = \mathbf{F} \quad (3.31)$$

where, \mathbf{K} is the global stiffness matrix, \mathbf{M} is the global mass matrix, \mathbf{B} is the global boundary matrix, \mathbf{F} is the global load vector. The above system of equations was assembled and solved in MATLAB, a sparse solver was written, which utilized the symmetric banded structure of these matrices.

For numerical quadrature the element coordinates are parameterized by natural coordinates, $-1 \leq \xi \leq 1, -1 \leq \eta \leq 1$. For the four node element the corner node points defined in natural coordinates are, (see Figure 3.2):

$$\begin{aligned}(\xi_1, \eta_1) &= (-1, -1) \\(\xi_2, \eta_2) &= (1, -1) \\(\xi_3, \eta_3) &= (1, 1) \\(\xi_4, \eta_4) &= (-1, 1)\end{aligned}$$

The global coordinates (x, y) are related to the element natural coordinates (ξ, η) by,

$$\begin{aligned}x(\xi, \eta) &= \sum_{i=1}^4 N_i^e(\xi, \eta) x_i^e, \\y(\xi, \eta) &= \sum_{i=1}^4 N_i^e(\xi, \eta) y_i^e.\end{aligned}\tag{3.32}$$

The relation between physical and natural derivatives is given by,

$$\begin{bmatrix} \frac{\partial N_i}{\partial x} \\ \frac{\partial N_i}{\partial y} \end{bmatrix} = \mathbf{J}^{-1} \begin{bmatrix} \frac{\partial N_i}{\partial \xi} \\ \frac{\partial N_i}{\partial \eta} \end{bmatrix}\tag{3.33}$$

where

$$\mathbf{J} = \begin{bmatrix} \frac{\partial x}{\partial \xi} & \frac{\partial y}{\partial \xi} \\ \frac{\partial x}{\partial \eta} & \frac{\partial y}{\partial \eta} \end{bmatrix}\tag{3.34}$$

is the Jacobian matrix. For square elements with edge length h^e , the Jacobian matrix simplifies to,

$$\mathbf{J} = \begin{bmatrix} \frac{h^e}{2} & 0 \\ 0 & \frac{h^e}{2} \end{bmatrix}\tag{3.35}$$

resulting in a constant determinant,

$$J^e = \det(\mathbf{J}) = \frac{(h^e)^2}{4}. \quad (3.36)$$

Based on this mapping, equation 3.23 may be written in natural coordinates as,

$$\mathbf{B}^e = \mathbf{J}^{-1} \begin{bmatrix} N_{1,\xi} & N_{2,\xi} & N_{3,\xi} & N_{4,\xi} \\ N_{1,\eta} & N_{2,\eta} & N_{3,\eta} & N_{4,\eta} \end{bmatrix}. \quad (3.37)$$

Using a change of variable,

$$\int_{\Omega^e} f(x, y) dx dy = \int_{-1}^1 \int_{-1}^1 f(\xi, \eta) J^e d\xi d\eta \quad (3.38)$$

the element matrices in natural coordinates are,

$$\mathbf{k}^e = \int_{-1}^1 \int_{-1}^1 \mathbf{B}^{eT} \mathbf{B}^e J^e d\xi d\eta \quad (3.39)$$

$$\mathbf{m}^e = \int_{-1}^1 \int_{-1}^1 \mathbf{N}^{eT} \mathbf{N}^e J^e d\xi d\eta \quad (3.40)$$

$$\begin{aligned} \mathbf{b}^e = & \left(\int_{-1}^1 \mathbf{N}^{eT} \mathbf{N}^e \frac{h^e}{2} d\xi \right)_{\eta=-1} + \left(\int_{-1}^1 \mathbf{N}^{eT} \mathbf{N}^e \frac{h^e}{2} d\eta \right)_{\xi=1} + \left(\int_{-1}^1 \mathbf{N}^{eT} \mathbf{N}^e \frac{h^e}{2} d\xi \right)_{\eta=1} \\ & + \left(\int_{-1}^1 \mathbf{N}^{eT} \mathbf{N}^e \frac{h^e}{2} d\eta \right)_{\xi=-1} \end{aligned} \quad (3.41)$$

$$\begin{aligned} \mathbf{f}^e = & \left(\int_{-1}^1 \mathbf{N}^{eT} g_1 \frac{h^e}{2} d\xi \right)_{\eta=-1} + \left(\int_{-1}^1 \mathbf{N}^{eT} g_2 \frac{h^e}{2} d\eta \right)_{\xi=1} + \left(\int_{-1}^1 \mathbf{N}^{eT} g_3 \frac{h^e}{2} d\xi \right)_{\eta=1} \\ & + \left(\int_{-1}^1 \mathbf{N}^{eT} g_4 \frac{h^e}{2} d\eta \right)_{\xi=-1}. \end{aligned} \quad (3.42)$$

The arrays are evaluated using numerical quadrature,

$$\mathbf{k}^e = \sum_{a,b=1}^2 \mathbf{B}^{eT}(\xi_a, \eta_b) \mathbf{B}^e(\xi_a, \eta_b) J^e w_a w_b \quad (3.43)$$

$$\mathbf{m}^e = \sum_{a,b=1}^2 \mathbf{N}^{e^T}(\xi_a, \eta_b) \mathbf{N}^e(\xi_a, \eta_b) J^e w_a w_b \quad (3.44)$$

$$\begin{aligned} \mathbf{b}^e = & \sum_{a=1}^p \mathbf{N}^{e^T}(\xi_a) \mathbf{N}^e(\xi_a) \frac{h^e}{2} w_a \Big|_{\eta=-1} + \sum_{b=1}^p \mathbf{N}^{e^T}(\eta_b) \mathbf{N}^e(\eta_b) \frac{h^e}{2} w_b \Big|_{\xi=1} \\ & + \sum_{a=1}^p \mathbf{N}^{e^T}(\xi_a) \mathbf{N}^e(\xi_a) \frac{h^e}{2} w_a \Big|_{\eta=1} + \sum_{b=1}^p \mathbf{N}^{e^T}(\eta_b) \mathbf{N}^e(\eta_b) \frac{h^e}{2} w_b \Big|_{\xi=-1} \end{aligned} \quad (3.45)$$

$$\begin{aligned} \mathbf{f}^e = & \sum_{a=1}^p \mathbf{N}^{e^T}(\xi_a) g_1 \frac{h^e}{2} w_a \Big|_{\eta=-1} + \sum_{b=1}^p \mathbf{N}^{e^T}(\eta_b) g_2 \frac{h^e}{2} w_b \Big|_{\xi=1} \\ & + \sum_{a=1}^p \mathbf{N}^{e^T}(\xi_a) g_3 \frac{h^e}{2} w_a \Big|_{\eta=1} + \sum_{b=1}^p \mathbf{N}^{e^T}(\eta_b) g_4 \frac{h^e}{2} w_b \Big|_{\xi=-1} \end{aligned} \quad (3.46)$$

where, (ξ_a, η_b) are the quadrature points and (w_a, w_b) are the weights. In order to enforce the boundary conditions accurately, the element boundary matrix \mathbf{b}^e and the element traction vector \mathbf{f}^e are evaluated using ten point Gauss quadrature rules ($p = 10$). For the element mass and stiffness matrices two point quadrature rules are used. The following quadrature rules are considered,

Gauss quadrature:

$$\begin{aligned} \xi_1 &= -\xi_2 = \frac{1}{\sqrt{3}}, \\ \eta_1 &= -\eta_2 = \frac{1}{\sqrt{3}}, \\ w_1 &= w_2 = 1. \end{aligned} \quad (3.47)$$

Lobatto quadrature (Trapezoidal rule):

$$\begin{aligned} \xi_1 &= -\xi_2 = 1, \\ \eta_1 &= -\eta_2 = 1, \\ w_1 &= w_2 = 1. \end{aligned} \quad (3.48)$$

Spectral quadrature:

$$\begin{aligned}\xi_1 &= -\xi_2 = \sqrt{\frac{2}{3}}, \\ \eta_1 &= -\eta_2 = \sqrt{\frac{2}{3}}, \\ w_1 &= w_2 = 1.\end{aligned}\tag{3.49}$$

For comparison, different quadrature rules are used for stiffness and mass matrices, see Table II.

Table 3.1

Quadrature Rules Used on Stiffness and Mass Matrices.

Method	Stiffness (\mathbf{k}^e)	Mass (\mathbf{m}^e)
Galerkin	Gauss	Gauss
Galerkin-LM	Gauss	Lobatto
Galerkin-HM	Gauss	Spectral
Spectral	Spectral	Spectral
Spectral-LM	Spectral	Lobatto

(a) Galerkin

The element stiffness and mass matrices evaluated using Gauss quadrature rules results in the standard Galerkin method. In this case the stiffness and mass matrices are exactly evaluated and the mass is referred to as *consistent mass*.

(b) Galerkin-Lumped/Diagonal Mass (Galerkin-LM)

The element stiffness matrix is evaluated exactly using Gauss quadrature while the mass matrix is evaluated using Lobatto quadrature rules resulting in the Galerkin method with lumped mass. In this case the mass matrix is diagonal and is referred to as the *lumped mass*.

(c) Galerkin-High Order Mass (Galerkin-HM)

The element stiffness matrix is evaluated exactly using Gauss quadrature while the element mass matrix is evaluated with Spectral quadrature resulting in the Galerkin method with high order mass. The element mass matrix is higher order accurate for waves propagating along mesh lines and is referred to as *high order mass*.

(d) Spectral Element (Spectral)

Both the mass and stiffness matrices are evaluated using spectral quadrature rules resulting in the high order accurate spectral element.

(e) Spectral Element with Lumped Mass (Spectral-LM)

The stiffness matrix is evaluated using Spectral quadrature rules while the mass matrix is evaluated using Lobatto quadrature rules resulting in the Spectral element with lumped mass.

3.2.5 Galerkin Least Squares Method (GLS)

Numerical results are also compared for modified Galerkin methods. In the GLS method, a least-squares operator is added to equation 3.10. The additional operator is constructed from the residual of the governing differential equation evaluated within

element interiors, Harari [1991]. Formally, GLS can be stated as, Find $\phi^h(x, y)$, such that for all $w^h(x, y)$,

$$A_{GLS}(w^h, \phi^h) = L_{GLS}(w^h) \quad (3.50)$$

where

$$A_{GLS}(w^h, \phi^h) = A(w^h, \phi^h) + \sum_{e=1}^n \int_{\Omega^e} \tau (\nabla^2 w^h + k^2 w^h)(\nabla^2 \phi^h + k^2 \phi^h) d\Omega \quad (3.51)$$

and for source term $f=0$,

$$L_{GLS}(w^h) = L(w^h). \quad (3.52)$$

In the above, $\tau(k, h)$ is a frequency (wavenumber) and element size dependent mesh parameter with units of inverse length-squared, determined from dispersion analysis. If $\tau = 0$, the method reverts to the standard Galerkin method. Assuming τ independent of (x, y) and bi-linear elements, the GLS method becomes,

$$\int_{\Omega} \nabla w^h \cdot \nabla \phi^h d\Omega - \gamma \int_{\Omega} w^h \phi^h d\Omega + ik \int_{\Gamma} w^h \phi^h d\Gamma = \int_{\Gamma} w^h g d\Gamma \quad (3.53)$$

where

$$\gamma = k^2 (1 - \tau k^2) \quad (3.54)$$

is a modified wavenumber.

Several choices for τ are possible. Thompson and Pinsky [1995] derived a τ which is dependent on k and h , yet independent of coordinates (x, y) , which minimizes dispersion error for all wave vector orientations θ :

$$\tau k^2 = 1 - \frac{6(4 - f_x - f_y - 2f_x f_y)}{(kh)^2 (2 + f_x)(2 + f_y)} \quad (3.55)$$

where

$$\begin{aligned} f_x &= \cos(kh \cos \frac{\pi}{8}), \\ f_y &= \cos(kh \sin \frac{\pi}{8}). \end{aligned} \quad (3.56)$$

Using exact integration and after assembly the following linear system of equations is obtained,

$$(\mathbf{K} - k^2 \mathbf{M}_{GLS} + ik \mathbf{B})\mathbf{d} = \mathbf{F} \quad (3.57)$$

where, $\mathbf{M}_{GLS} = (1 - \tau k^2) \mathbf{M}$.

3.2.6 Quasi Stabilized Finite Element Method (QSFEM)

The QSFEM is derived by optimizing the Generalized Finite Element method (GFEM), Babuska et.al. [1995]. The GFEM was first introduced by Babuska and Osborn [1983]. In this method, local mappings are introduced which transform the usual finite element basis functions to another local basis. These local mappings are designed in such way that the resulting method applied to a differential equation converges with an optimal rate. It defines a $n \times n$ matrix \mathbf{A} , and a linear mapping L , which maps the right hand side of equation 3.2 onto the vector of the right hand side \mathbf{b} , resulting in the matrix problem,

$$\mathbf{A}\mathbf{d} = \mathbf{b} \quad (3.58)$$

A typical internal node (grid point), denoted $d_{m,n}$, is associated with one equation of the form,

$$\begin{aligned} &A_2 d_{m-1,n+1} + A_1 d_{m,n+1} + A_2 d_{m+1,n+1} \\ &A_1 d_{m-1,n} + A_0 d_{m,n} + A_1 d_{m+1,n} \\ &A_2 d_{m-1,n-1} + A_1 d_{m,n-1} + A_2 d_{m+1,n-1}. \end{aligned} \quad (3.59)$$

The nine coefficients of this stencil are represented by a 3x3 array,

$$\begin{bmatrix} A_2 & A_1 & A_2 \\ A_1 & A_0 & A_1 \\ A_2 & A_1 & A_2 \end{bmatrix}. \quad (3.60)$$

Babuska et.al. [1995], derived the QSFEM for a uniform square mesh. Optimal values for A_0, A_1, A_2 were derived based on a Taylor series expansion of these coefficients in terms of kh , resulting in,

$$\begin{aligned} A_0 &= 4 \\ A_1 &= 2 \frac{c_1(\alpha)s_1(\alpha) - c_2(\alpha)s_2(\alpha)}{c_2(\alpha)s_2(\alpha)(c_1(\alpha) + s_1(\alpha)) - c_1(\alpha)s_1(\alpha)(c_2(\alpha) + s_2(\alpha))} \\ A_2 &= \frac{c_2(\alpha) + s_2(\alpha) - c_1(\alpha) - s_1(\alpha)}{c_2(\alpha)s_2(\alpha)(c_1(\alpha) + s_1(\alpha)) - c_1(\alpha)s_1(\alpha)(c_2(\alpha) + s_2(\alpha))}, \end{aligned} \quad (3.61)$$

where,

$$\begin{aligned} c_1(\alpha) &= \cos(\alpha \cos \frac{\pi}{16}) & s_1(\alpha) &= \cos(\alpha \sin \frac{\pi}{16}) \\ c_2(\alpha) &= \cos(\alpha \cos \frac{3\pi}{16}) & s_2(\alpha) &= \cos(\alpha \sin \frac{3\pi}{16}) \end{aligned} \quad (3.62)$$

and $\alpha = kh$. The system matrix \mathbf{A} is a complicated function of $k = \omega / c$, and thus the QSFEM cannot be used directly for transient analysis. The discretization of the boundary conditions and the assembly of the load vector \mathbf{b} is accomplished using a finite difference scheme described in Elliptical Differential Equations [1992]. Normal derivatives on edge boundaries are represented by a symmetric difference formula centered at edge points. For example, for a typical node $d_{m,n}$ located on the bottom edge Γ_1 , see Figure 3.3, the normal derivative is represented by,

$$\frac{\partial \phi}{\partial n} = \frac{\partial \phi}{\partial y} = \frac{1}{2h} [d_{m,n+1} - d_{m,n-1}]. \quad (3.63)$$

Similarly, the normal derivatives for neighboring edge points $d_{m-1,n}$ and $d_{m+1,n}$ are given by,

$$\frac{\partial\phi}{\partial n} = \frac{\partial\phi}{\partial y} = \frac{1}{2h} [d_{m-1,n+1} - d_{m-1,n-1}] \quad (3.64)$$

$$\frac{\partial\phi}{\partial n} = \frac{\partial\phi}{\partial y} = \frac{1}{2h} [d_{m+1,n+1} - d_{m+1,n-1}] \quad (3.65)$$

respectively. Node points $d_{m-1,n-1}$, $d_{m,n-1}$, $d_{m+1,n-1}$ lie outside the domain Ω , and are referred to as fictitious nodes. Applying the non-reflecting boundary condition,

$$\frac{\partial\phi}{\partial y} = -g_1 + ik\phi \quad \text{on } \Gamma_1 \quad (3.66)$$

for edge node $d_{m,n}$ gives,

$$\frac{1}{2h} [d_{m,n+1} - d_{m,n-1}] = -g_{1(m,n)} + ikd_{m,n} \quad (3.67)$$

which can be rearranged in terms of the fictitious node as,

$$d_{m,n-1} = 2h[g_{1(m,n)} - ikd_{m,n}] + d_{m,n+1} \quad (3.68)$$

Similar expressions can be derived for the other two fictitious points, i.e.

$$d_{m-1,n-1} = 2h[g_{1(m-1,n)} - ikd_{m-1,n}] + d_{m-1,n+1} \quad (3.69)$$

$$d_{m+1,n-1} = 2h[g_{1(m+1,n)} - ikd_{m+1,n}] + d_{m+1,n+1} \quad (3.70)$$

The three fictitious points are eliminated by substituting equations 3.68, 3.69, 3.70 into the nine-point difference stencil, equation 3.59, associated with bottom edge node $d_{m,n}$,

resulting in the modified stencil,

$$\begin{bmatrix} 2A_2 & 2A_1 & 2A_2 \\ (A_1 + 2ikhA_2)(A_0 + 2ikhA_1) & (A_1 + 2ikhA_2) & \\ 0 & 0 & 0 \end{bmatrix} \quad (3.71)$$

with RHS terms added to the load vector,

$$2h[A_2g_{1(m-1,n)} + A_1g_{1(m,n)} + A_2g_{1(m+1,n)}]. \quad (3.72)$$

Similar modified stencils and load terms are derived for nodes on the other three edges,

i.e., on Γ_2

$$\begin{bmatrix} 2A_2 (A_1 + 2ikhA_2) & 0 \\ 2A_1 (A_0 + 2ikhA_1) & 0 \\ 2A_2 (A_1 + 2ikhA_2) & 0 \end{bmatrix}, \quad 2h \begin{bmatrix} A_2g_{2(m,n+1)} \\ A_1g_{2(m,n)} \\ A_2g_{2(m,n-1)} \end{bmatrix} \quad (3.73)$$

on Γ_3

$$\begin{bmatrix} 0 & 0 & 0 \\ (A_1 + 2ikhA_2)(A_0 + 2ikhA_1) & (A_1 + 2ikhA_2) & \\ 2A_2 & 2A_1 & 2A_2 \end{bmatrix}, \quad 2h \begin{bmatrix} A_2g_{3(m-1,n)} \\ A_1g_{3(m,n)} \\ A_2g_{3(m+1,n)} \end{bmatrix} \quad (3.74)$$

on Γ_4

$$\begin{bmatrix} 0 (A_1 + 2ikhA_2) & 2A_2 \\ 0 (A_0 + 2ikhA_1) & 2A_1 \\ 0 (A_1 + 2ikhA_2) & 2A_2 \end{bmatrix}, \quad 2h \begin{bmatrix} A_2g_{4(m,n+1)} \\ A_1g_{4(m,n)} \\ A_2g_{4(m,n-1)} \end{bmatrix}. \quad (3.75)$$

The stencil for the corner-nodes involves five fictitious nodes that don't lie in the domain, see Figure 3.4. These points are expressed in terms of the interior nodes by representing the normal derivatives on the intersecting edges by a symmetric difference scheme and relating them to the non-reflecting boundary conditions on those edges,

similar to the procedure adapted for the edge nodes. For example for a typical corner node $d_{m,n}$, the fictitious nodes, $d_{m-1,n+1}$, $d_{m-1,n}$, $d_{m,n-1}$, $d_{m+1,n-1}$ can be expressed as,

$$d_{m-1,n+1} = d_{m+1,n+1} - 2h[g_{4(m,n+1)} - ikd_{(m,n+1)}] \quad (3.76)$$

$$d_{m-1,n} = d_{m+1,n} - 2h[g_{4(m,n)} - ikd_{(m,n)}] \quad (3.77)$$

$$d_{m,n-1} = d_{m,n+1} - 2h[g_{1(m,n)} - ikd_{(m,n)}] \quad (3.78)$$

$$d_{m+1,n-1} = d_{m+1,n+1} - 2h[g_{1(m+1,n)} - ikd_{(m+1,n)}] \quad (3.79)$$

respectively. For the fictitious node $d_{m-1,n-1}$, a zero coefficient is assumed as it cannot be expressed in terms of the interior nodes. Substituting this condition and equations 3.76, 3.77, 3.78 and 3.79 into the nine-point difference stencil, the modified stencil for the bottom left corner node, can be written as,

$$\begin{bmatrix} 0 & (2A_1 - 4ikhA_2) & 3A_2 \\ 0 & (A_0 - 4ikhA_1) & (2A_1 - 2ikhA_2) \\ 0 & 0 & 0 \end{bmatrix}, \quad (3.80)$$

with RHS term added to the load vector,

$$-2h \begin{bmatrix} A_2 g_{4(m,n-1)} \\ (A_1 - 2ikhA_2) g_{1(m,n)} + A_1 g_{4(m,n)} \\ A_2 g_{4(m,n+1)} \\ 2A_2 g_{1(m+1,n)} \end{bmatrix}. \quad (3.81)$$

Similar modified stencils and load terms are derived for the other three corner nodes, i.e.

for the bottom right corner node,

$$\begin{bmatrix} 3A_2 & (2A_1 - 2ikhA_2) & 0 \\ (2A_1 - 2ikhA_2) & (A_0 - 4ikhA_1) & 0 \\ 0 & 0 & 0 \end{bmatrix}$$

$$-2h \begin{bmatrix} 2A_2 g_{1(m-1,n)} \\ A_2 g_{2(m,n-1)} \\ (A_1 - 2ikhA_2)g_{1(m,n)} + A_1 g_{2(m,n)} \\ A_2 g_{2(m,n+1)} \end{bmatrix} \quad (3.82)$$

for the top right corner node,

$$\begin{bmatrix} 0 & 0 & 0 \\ (2A_1 - 2ikhA_2) & (A_0 - 4ikhA_1) & 0 \\ 3A_2 & (2A_1 - 2ikhA_2) & 0 \end{bmatrix} -2h \begin{bmatrix} A_2 g_{3(m-1,n)} \\ 2A_2 g_{2(m,n-1)} \\ (A_1 - 2ikhA_2)g_{2(m,n)} + A_1 g_{3(m,n)} \\ A_2 g_{3(m+1,n)} \end{bmatrix} \quad (3.83)$$

and for the top left corner node,

$$\begin{bmatrix} 0 & 0 & 0 \\ 0 & (A_0 - 4ikhA_1) & (2A_1 - 2ikhA_2) \\ 0 & (2A_1 - 2ikhA_2) & 3A_2 \end{bmatrix} -2h \begin{bmatrix} A_2 g_{3(m-1,n)} \\ 2A_2 g_{4(m,n-1)} \\ (A_1 - 2ikhA_2)g_{4(m,n)} + A_1 g_{3(m,n)} \\ A_2 g_{3(m+1,n)} \end{bmatrix}. \quad (3.84)$$

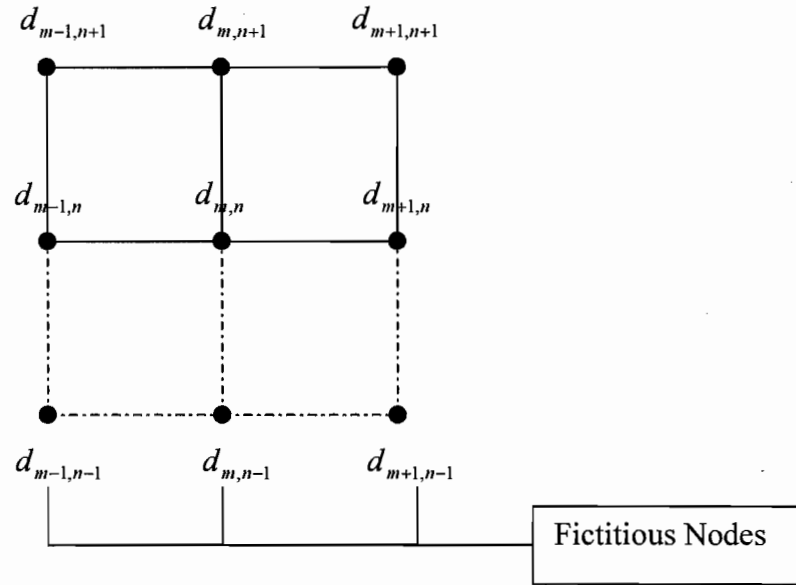


Figure 3.3 Stencil for edge nodes.

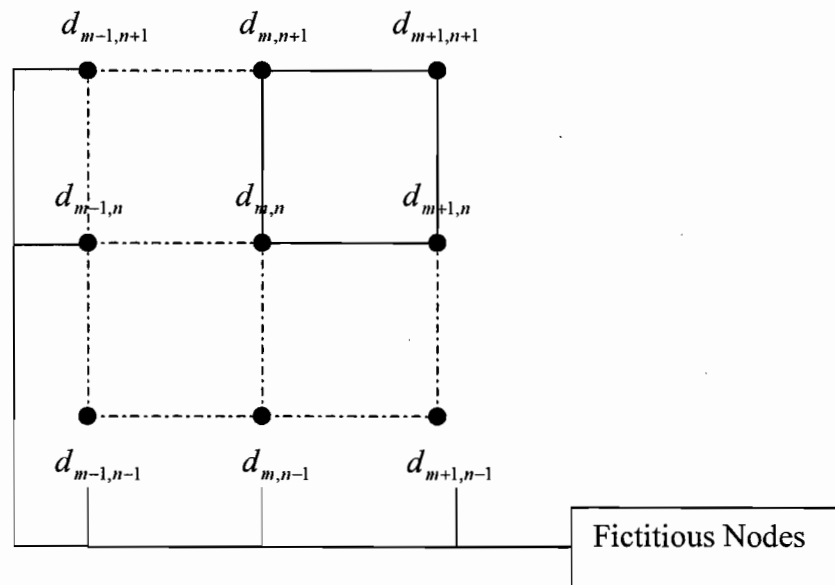


Figure 3.4 Stencil for corner nodes.

3.3 Numerical Results

In this section the accuracy of the different methods discussed above are compared. The *pollution effects* and *convergence rates* of these methods are also discussed.

Figure 3.5 shows the real component of the solution along the bottom edge Γ_1 for $\theta = 45^\circ$, and eight elements per wavelength. It can be seen that for the same number of elements per wavelength the Galerkin method using Gauss quadrature on both stiffness and mass shows significant phase error while the Spectral method accurately approximates the exact solution. In the following the accuracy is measured using the relative L_2 -norm and H_1 -seminorm defined as,

$$e_0 = \frac{\|\phi - \phi^h\|_0}{\|\phi\|_0} \quad (3.85)$$

$$e_1 = \frac{\|\phi - \phi^h\|_1}{\|\phi\|_1} \quad (3.86)$$

where,

$$\|\phi\|_0^2 = \int_{\Omega} \phi(x, y) \bar{\phi}(x, y) d\Omega = \sum_{e=1}^n \int_{\Omega^e} \phi \bar{\phi} d\Omega^e \quad (3.87)$$

$$\|\phi\|_1^2 = \int_{\Omega} \nabla \phi(x, y) \bullet \nabla \bar{\phi}(x, y) d\Omega = \sum_{e=1}^n \int_{\Omega^e} \nabla \phi \bullet \nabla \bar{\phi} d\Omega^e \quad (3.88)$$

and the over bar indicates complex conjugate.

In Figure 3.6, the error measured in H_1 -seminorm is plotted as a function of plane wave orientation angle θ , with fixed normalized wavenumber $kh = 0.75$, corresponding to eight elements per wavelength. Results are plotted over the range $0 \leq \theta \leq 45^\circ$, since the

solution is symmetric about $\theta = 45^\circ$. The results show the error using the Galerkin method is significantly larger than the Spectral, GLS, and QSFEM methods. The Spectral and QSFEM have similar accuracy, while the GLS error increases slightly at $\theta = 45^\circ$.

An interesting observation is that the Galerkin, Spectral, and QSFEM solutions are the most accurate along mesh diagonals corresponding to $\theta = 45^\circ$, while the solutions exhibit largest errors along the mesh lines, $\theta = 0^\circ$.

In Figure 3.7 the accuracy of different modified Galerkin methods is compared. The largest error is shown for the Lumped mass cases. The error in solution using the Galerkin method with Lumped mass, denoted Galerkin-LM, increases significantly for waves along mesh diagonals, $\theta = 45^\circ$, while the error using Spectral method with Lumped mass remains nearly constant over all angles θ , i.e. the Spectral-LM remains nearly anisotropic as observed from the dispersion equations. Along mesh lines at $\theta = 0^\circ$, the error of the Galerkin high-order mass, denoted Galerkin-HO is equal to that of the spectral method as expected from the dispersion analysis. However for plane wave solutions along mesh diagonals, $\theta = 45^\circ$, the error using Galerkin-HO mass increases and is larger than the error in the Standard Galerkin solution.

The same behavior is also observed when the number of elements per wavelength is decreased from eight to five, as shown in Figures 3.8 and 3.9, where the error is plotted for a fixed normalized wavenumber $kh = 1.25$.

Figure 3.10 illustrates the improved accuracy of the spectral method over the standard Galerkin method. The results show that the accuracy of the Spectral method

using five elements per wavelength ($kh = 1.25$) is nearly the same as using eight elements per wavelength ($kh = 0.75$) for the Galerkin method.

Figure 3.11 shows the convergence of the Galerkin and Spectral methods compared to the nodal interpolant of the exact solution, as the number of elements n is increased for fixed $k = 30$. Results show the spectral method error decreasing rapidly with n , approaching the optimal convergence rate of the interpolant. In contrast, several hundred elements are needed for the Galerkin method to converge to the interpolant. These results show that the same accuracy can be obtained using the spectral method with fewer elements, resulting in lower computational expense.

The pollution effect in different methods is compared in Figures 3.12 and 3.13. For a fixed number of elements per wavelength corresponding to constant $kh = 1.25$, the error increases with increasing wavenumber, for all wave angles θ . However, this effect is negligible in the case of the spectral element method.

In Figures 3.14, and 3.15, the error measured in L_2 -norm is plotted as a function of plane wave orientation angle θ , with fixed normalized wavenumber, $kh = 0.75$, corresponding to eight elements per wavelength. It can be seen that the results are similar to those obtained for error measured in H_1 -seminorm. The Galerkin method has significantly larger error than the spectral, GLS and QSFEM methods. The spectral element and QSFEM have similar accuracy, while the GLS error increases slightly at $\theta = 0^\circ, 45^\circ$. For modified Galerkin methods, the largest error is shown for the lumped mass cases. The error of the Galerkin lumped mass increases significantly for $\theta = 45^\circ$, while the error for spectral lumped mass remains nearly anisotropic. Along mesh lines at

$\theta = 0^\circ$, the error of the Galerkin higher order mass is equal to that of the spectral method, but the error increases for plane wave solutions along mesh diagonals.

Figure 3.15 shows the convergence rates of the Galerkin and spectral methods, as the number of elements n is increased for fixed $k = 30$. Results show the spectral method error decreasing rapidly with n , while the Galerkin method converges at a slower rate.

The pollution effect in different methods, for error measured in L_2 -norm are compared in Figure 3.17. For a fixed number of elements per wavelength corresponding to constant $kh = 1.25$, the error increases with increasing wavenumber, for all wave angles θ . However, this effect is negligible in the case of the spectral element method.

In summary, the dispersion error for the spectral element method is decreased compared to competing modified Galerkin methods while minimizing pollution error for high wavenumber solutions.

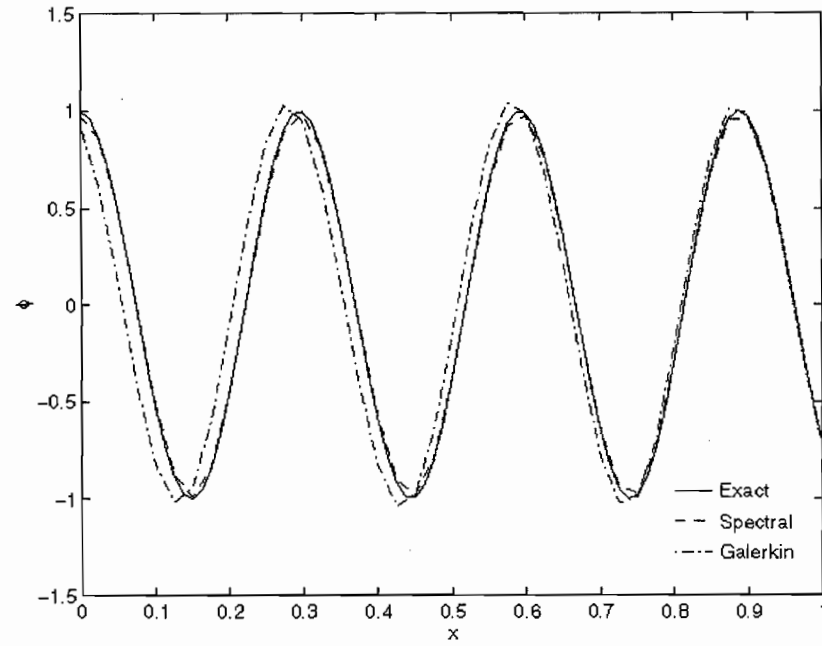


Figure 3.5 Real(ϕ) along the bottom edge, for $k = 30$, $kh = 0.75$, $\theta = 45$.
(8 elements per wave length)

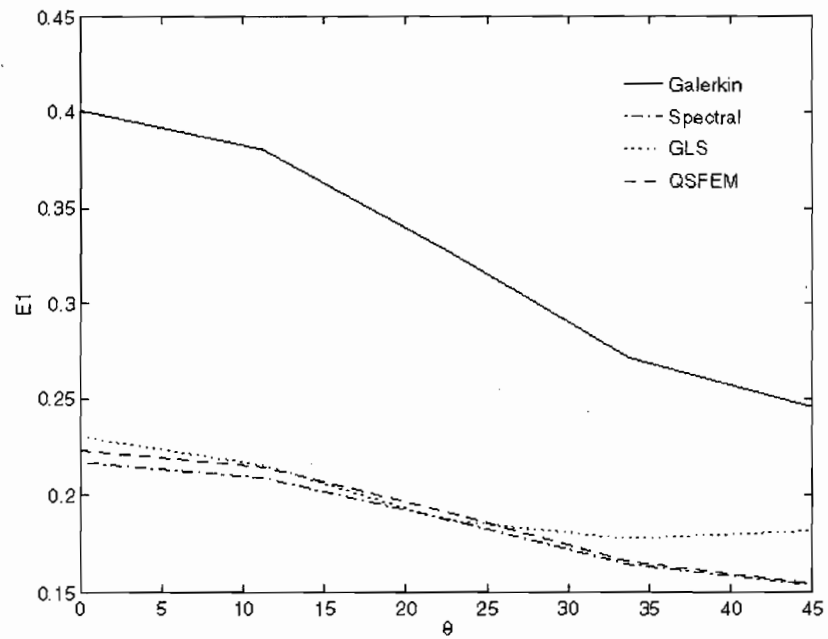


Figure 3.6 Error measured in H_1 -seminorm vs angle in degrees, for $k = 30$, $kh = 0.75$.

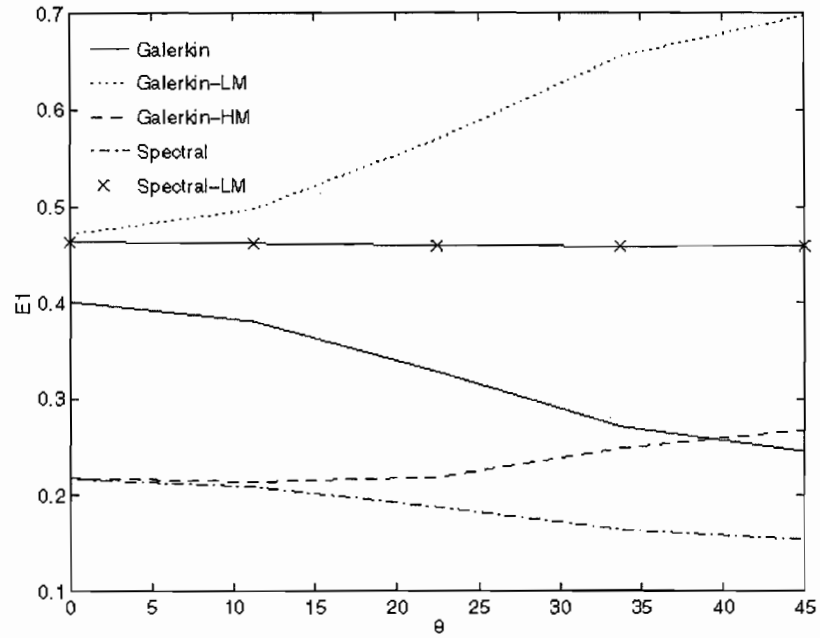


Figure 3.7 Error measured in H_1 -seminorm vs angle in degrees, for $k = 30$, $kh = 0.75$.

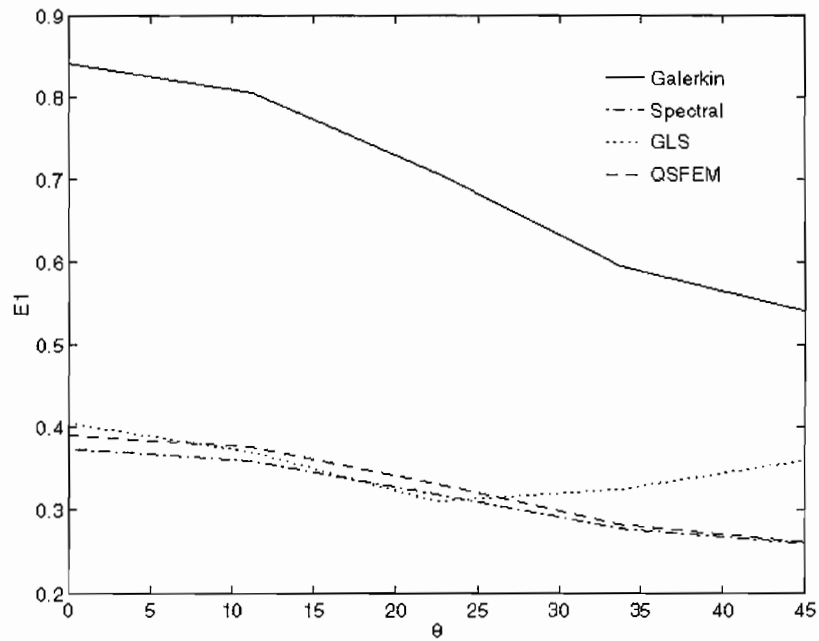


Figure 3.8 Error measured in H_1 -seminorm vs angle in degrees, for $k = 30$, $kh = 1.25$.
(5 elements per wave length)

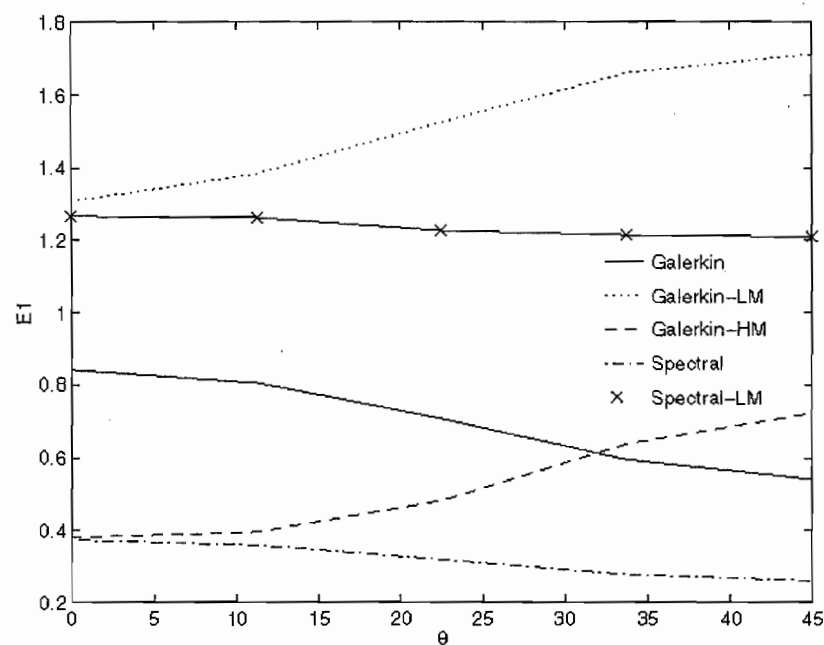


Figure 3.9 Error measured in H_1 -seminorm vs angle in degrees, for $k = 30$, $kh = 1.25$.

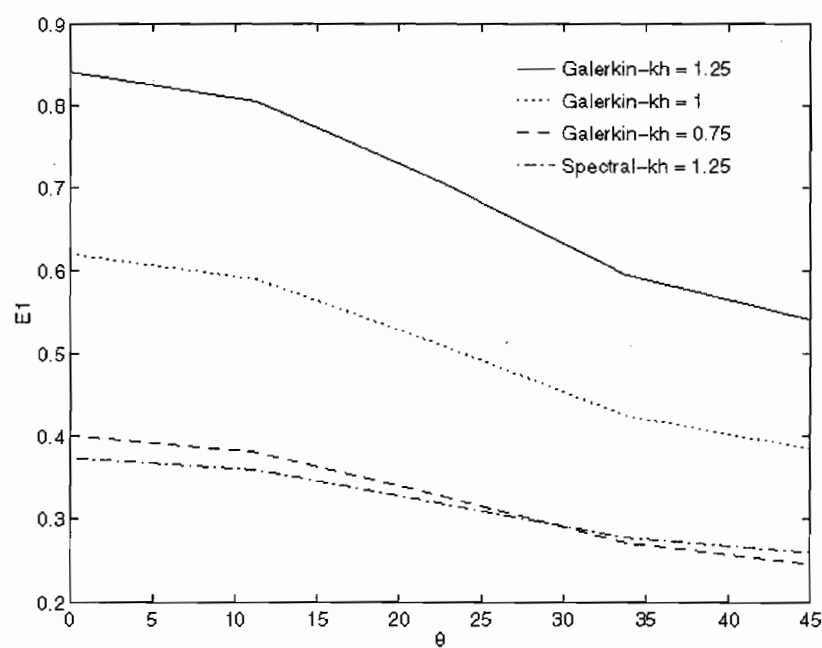


Figure 3.10 Comparison of error for Galerkin and Spectral methods, $k = 30$.

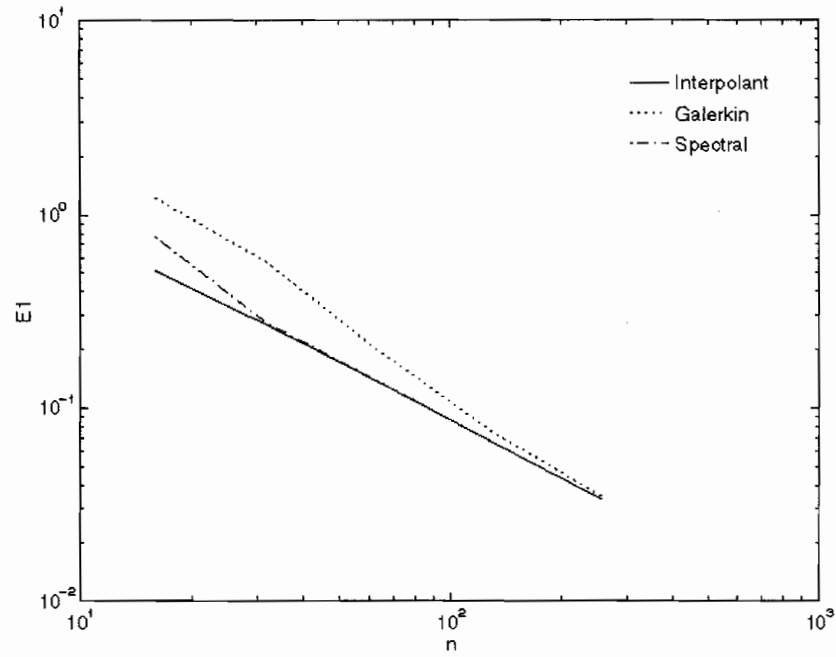


Figure 3.11 Convergence rates (slope = 1) measured in H_1 -seminorm.

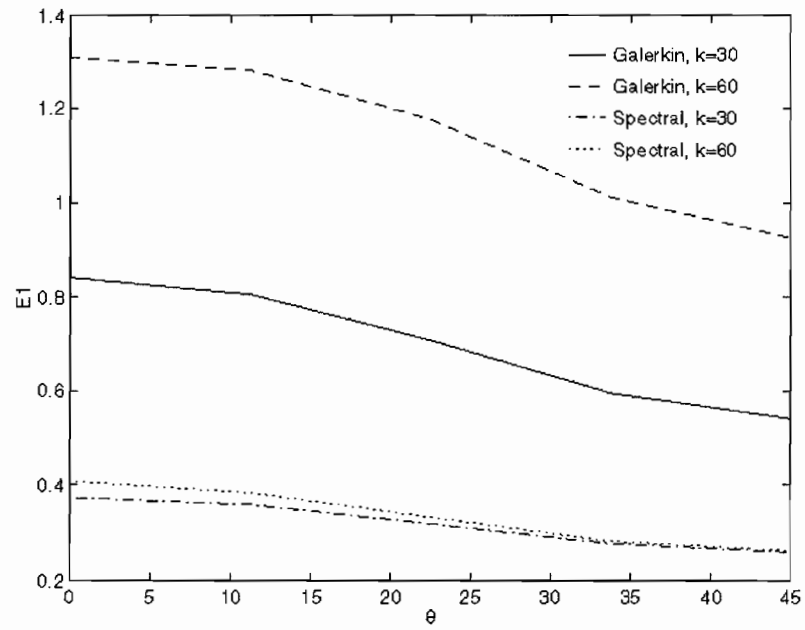


Figure 3.12 Pollution effect for $kh = 1.25$

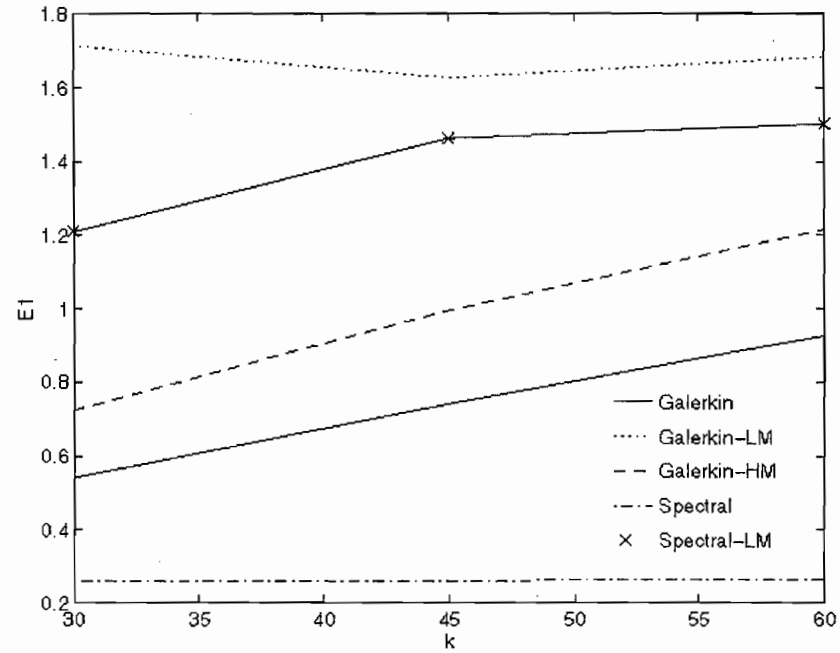


Figure 3.13 Pollution error for increasing wavenumber at $\theta = 45^\circ$ and $kh = 1.25$.

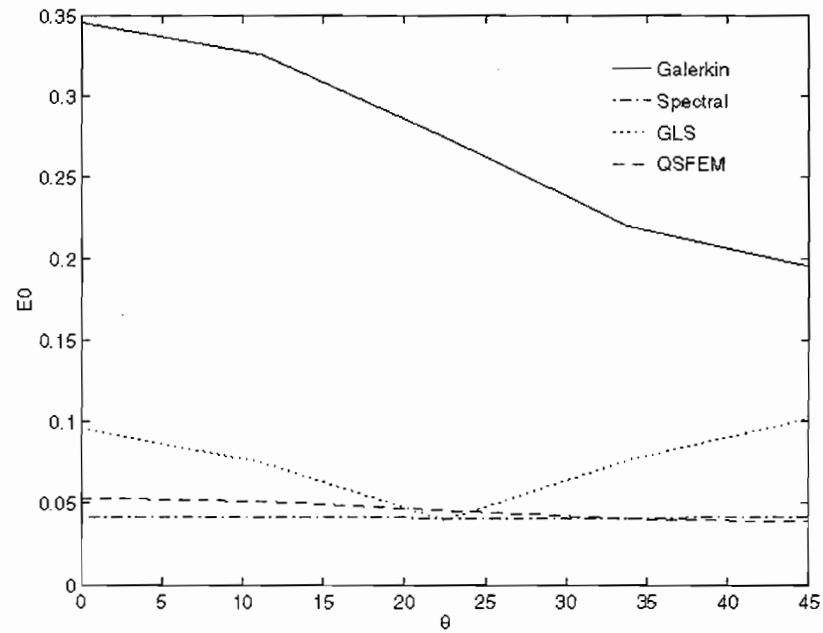


Figure 3.14 Error measured in L_2 -norm vs angle in degrees, for $k = 30$, $kh = 0.75$.
(8 elements per wave length)

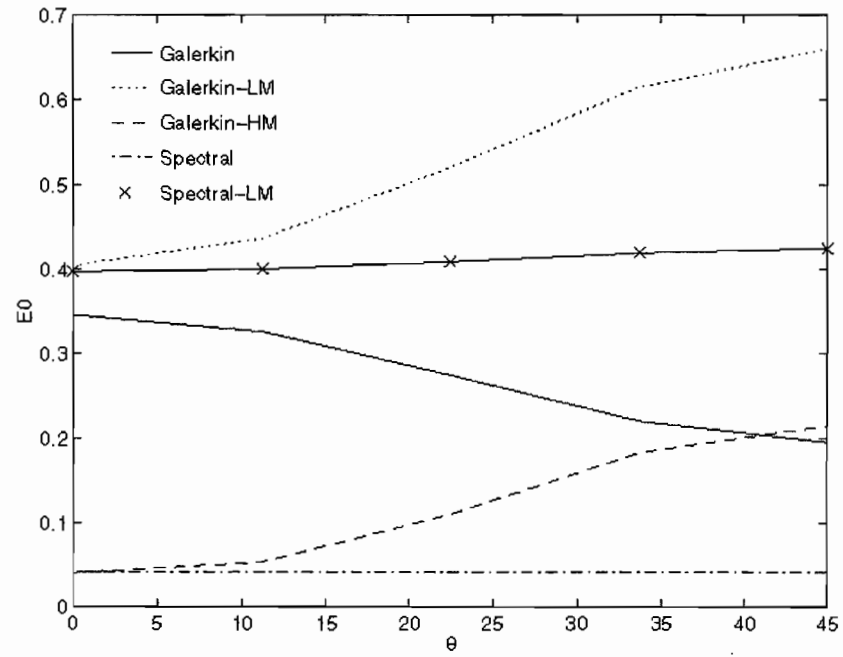


Figure 3.15 Error measured in L_2 -norm vs angle in degrees, for $k = 30$, $kh = 0.75$.

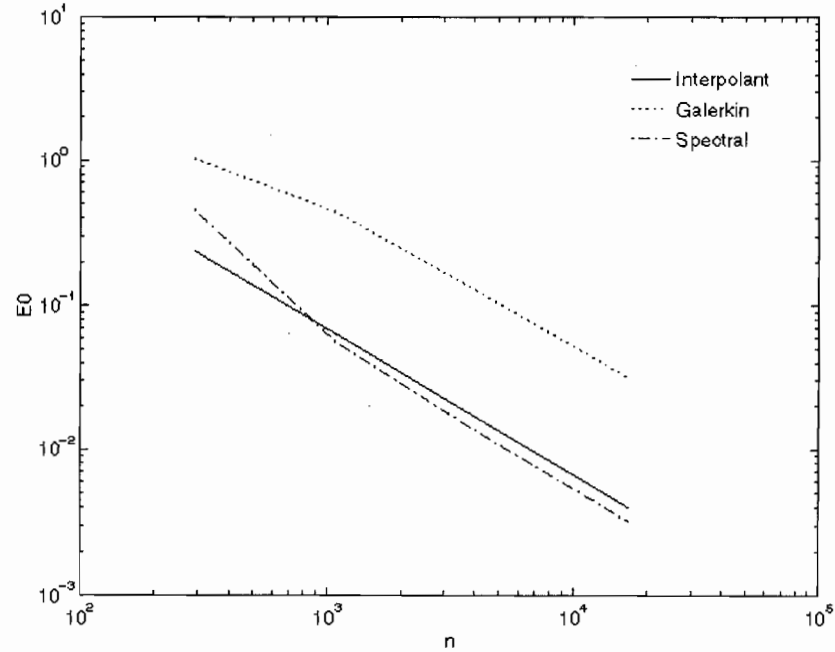


Figure 3.16 Convergence rates (slope = 2) measured in L_2 -norm.

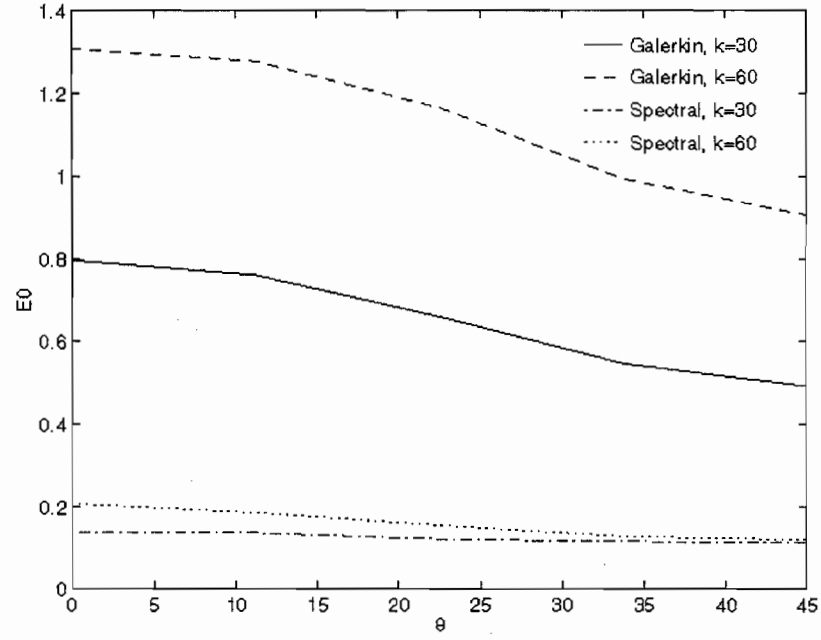


Figure 3.17 Pollution effect for $kh = 0.75$, error measured in L_2 -norm.

CHAPTER 4

HIGH-ORDER SPECTRAL ELEMENTS

4.1 Overview

In this chapter, optimal quadrature rules are derived for elements based on quadratic shape functions. For simplicity, one-dimensional dispersion analysis is used to derive quadrature rules which reduce dispersion. The quadrature rules obtained from one-dimensional analysis are then used for two-dimensional nine-node elements based on bi-quadratic Lagrange shape functions. Numerical results for the plane-wave model problem are used to compare the accuracy of bi-quadratic elements based on optimal quadrature rules derived in one-dimension with Galerkin, Galerkin lumped mass and GLS methods.

4.2 Design of High-Order Spectral Element

Consider the one-dimensional Helmholtz equation:

$$\nabla^2 \phi(x) + k^2 \phi(x) = -f \quad \text{in } \Omega \quad (4.1)$$

An exact solution of equation 4.1 is the plane-wave solution in one-dimension,

$$\phi(x) = A e^{i(kx)}. \quad (4.2)$$

The Galerkin equation corresponding to equation 4.1 is,

$$A(w^h, \phi^h) = L(w^h) \quad (4.3)$$

where

$$\begin{aligned} A(w^h, \phi^h) &= \int_{\Omega} \frac{\partial w^h}{\partial x} \frac{\partial \phi^h}{\partial x} dx - k^2 \int_{\Omega} w^h \phi^h dx \\ L(w^h) &= \int_{\Omega} w^h f dx \end{aligned} \quad (4.4)$$

where w^h is the weighting function and ϕ^h is the approximate solution. Consider a uniform mesh of one-dimensional, 3-node, quadratic elements, with element size h , see Figure 4.1. Let the element domain be parameterized over the local domain, $\xi \in (-1,1)$, with the usual mapping,

$$x(\xi) = L_1^e x_1^e + L_2^e x_2^e \quad (4.5)$$

where x_1^e, x_2^e are the nodal coordinates and L_1^e, L_2^e are the Lagrange interpolation functions,

$$L_1^e = \frac{1}{2}(1-\xi), \quad L_2^e = \frac{1}{2}(1+\xi). \quad (4.6)$$

For the above mapping the determinant of the Jacobian simplifies to,

$$J^e = \frac{h^e}{2}. \quad (4.7)$$

The finite element approximation of ϕ^h and w^h within each element is defined in terms of the nodal degrees of freedom as,

$$\phi^h(\xi) = \sum_{i=1}^3 N_i^e(\xi) d_i^e, \quad \xi \in (-1,1) \quad (4.8)$$

and

$$w^h(\xi) = \sum_{i=1}^3 N_i^e(\xi) w_i^e, \quad \xi \in (-1,1) \quad (4.9)$$

where $\phi_i^e = \phi^h(\xi_i)$ and $w_i^e = w^h(\xi_i)$ are the element nodal degrees of freedom and the quadratic interpolation functions are defined as,

$$\begin{aligned} N_1^e &= -\frac{1}{2}\xi(1-\xi) \\ N_2^e &= (1+\xi)(1-\xi) \\ N_3^e &= \frac{1}{2}\xi(1+\xi). \end{aligned} \quad (4.10)$$

Substituting equations 4.8 and 4.9 into equation 4.3 and assuming $f = 0$, leads to the 3x3 element dynamic stiffness array defined as a linear combination of static stiffness and mass matrices,

$$\mathbf{s}^e \mathbf{d}^e = (\mathbf{k}^e - k^2 \mathbf{m}^e) \mathbf{d}^e = \mathbf{0} \quad (4.11)$$

where,

$$k_{ij}^e = \int_{-1}^1 \frac{dN_i^e}{d\xi} \frac{dN_j^e}{d\xi} \frac{1}{J^e} d\xi \quad (4.12)$$

$$m_{ij}^e = \int_{-1}^1 N_i^e N_j^e J^e d\xi \quad (4.13)$$

For quadratic shape functions, three point quadrature is used to evaluate the stiffness and mass,

$$k_{ij}^e = \sum_{a=1}^3 \frac{dN_i^e(\xi_a)}{d\xi} \frac{dN_j^e(\xi_a)}{d\xi} \frac{1}{J^e} w_a \quad (4.14)$$

$$m_{ij}^e = \sum_{a=1}^3 N_i^e(\xi_a) N_j^e(\xi_a) J^e w_a. \quad (4.15)$$

The following assumptions are made on the quadrature rules,

$$w_1 = w_3 \quad \text{weights are symmetric} \quad (4.16)$$

$$\xi_1 = -\xi_3, \xi_2 = 0 \quad \text{points are symmetric} \quad (4.17)$$

$$w_1 + w_2 + w_3 = 2 \quad \text{to exactly integrate a constant.} \quad (4.18)$$

$$w_1 = \frac{1}{3\xi_1^2} \quad \text{to exactly integrate a quadratic expression.} \quad (4.19)$$

The three point Gauss quadrature rules are,

$$\begin{aligned} w_1 = w_3 = \frac{5}{9}, \quad w_2 = \frac{8}{9} \\ \xi_1 = -\xi_3 = -\sqrt{\frac{3}{5}}, \quad \xi_2 = 0. \end{aligned} \quad (4.20)$$

The three point Lobatto quadrature rules are,

$$\begin{aligned} w_1 = w_3 = 1/3, \quad w_2 = 4/3 \\ \xi_1 = -\xi_3 = -1, \quad \xi_2 = 0. \end{aligned} \quad (4.21)$$

Three point Gauss rules exactly integrate both stiffness and mass matrices, while Lobatto underintegrates and diagonalizes the mass matrix. Exact integration of the mass is referred to as consistent mass, while diagonal mass is called Lumped. After assembling element arrays for two adjacent elements, see Figure 4.2, the stencils for a typical interior node, denoted $n + 1/2$, and for a typical edge node, n , are determined to be,

$$\begin{aligned} n^{\text{th}} \text{ node :} \quad & s_{13}d_{n-1} + s_{12}d_{n-1/2} + 2s_{11}d_n + s_{12}d_{n+1/2} + s_{13}d_{n+1} = 0, \\ n + 1/2 \text{ node :} \quad & s_{13}d_n + s_{22}d_{n+1/2} + s_{12}d_{n+1}. \end{aligned} \quad (4.22)$$

Allowing for different amplitudes at the end nodes n , and element center nodes $n + 1/2$, plane wave solutions are assumed,

$$d_n = A_1 e^{ik^h n h}, \quad d_{n+1/2} = A_2 e^{ik^h (n+1/2)h}. \quad (4.23)$$

Substitution of equation 4.23 into equation 4.22, results in the symmetric characteristic

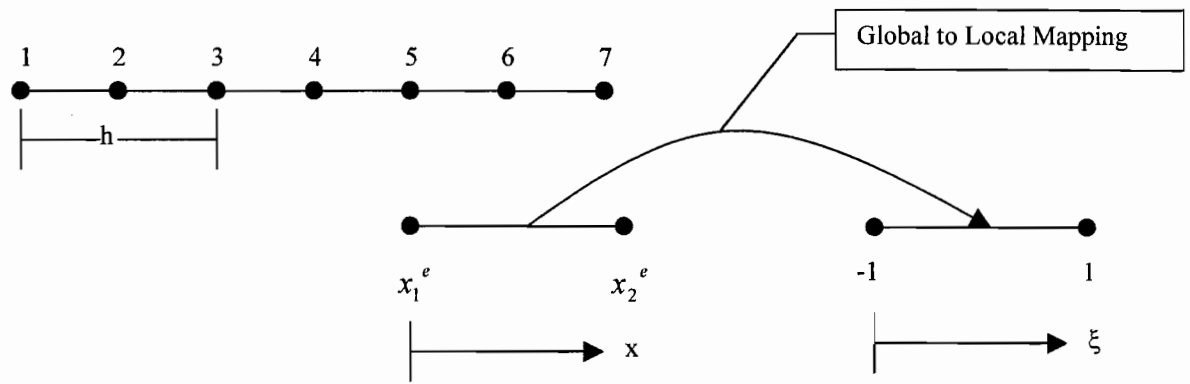


Figure 4.1 1-D Quadratic mesh

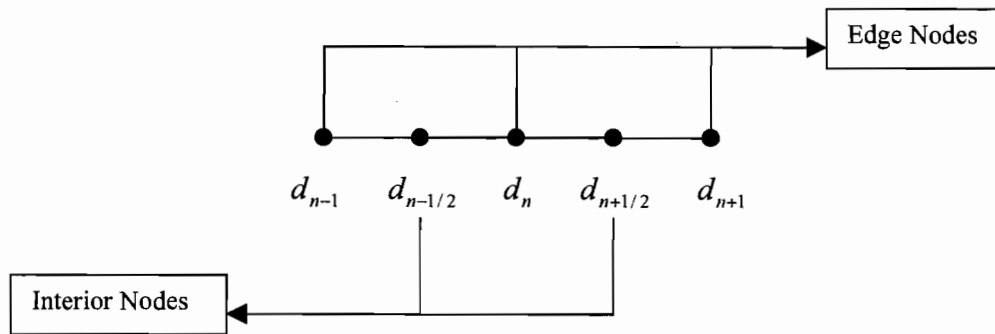


Figure 4.2 Stencil for 1-D quadratic mesh.

matrix that relates the normalized frequency $k = \omega / c$ with the numerical wave number k^h , Thompson and Pinsky [1994]

$$\begin{bmatrix} D_{11} & D_{12} \\ D_{12} & D_{22} \end{bmatrix} \begin{Bmatrix} A_1 \\ A_2 \end{Bmatrix} = \mathbf{0}. \quad (4.24)$$

The dispersion relation is obtained by setting the determinant of the characteristic matrix to zero, i.e.

$$D_{11}D_{22} - D_{12}^2 = 0. \quad (4.25)$$

Rearranging equation 4.25 leads to the characteristic equation,

$$k^h h = \cos^{-1} \left(\frac{-(s_{11}s_{22} - s_{12}^2)}{(s_{13}s_{22} - s_{12}^2)} \right). \quad (4.26)$$

Expanding equation 4.26 in a Taylor's series expansion of k , for consistent mass,

$$k^h h = kh - \frac{1}{1440}(kh)^5 + \frac{11}{302400}(kh)^7 + c_1(kh)^9 + \dots \quad (4.27)$$

for lumped mass,

$$k^h h = kh + \frac{1}{2880}(kh)^5 + \frac{1}{96768}(kh)^7 + c_2(kh)^9 + \dots \quad (4.28)$$

From equations 4.27 and 4.28 it can be seen that the mass matrix which annihilates the fifth order term corresponds to,

$$m^e = \frac{1}{3}m_c^e + \frac{2}{3}m_l^e. \quad (4.29)$$

where, m_c^e is the element consistent mass matrix, and m_l^e is the element lumped mass matrix. This special mass matrix that results in higher-order accuracy can be obtained by

using the quadrature rules,

$$\begin{aligned}\xi_1 = -\xi_3 = -\sqrt{13/15}, \xi_2 = 0 \\ w_1 = w_3 = 5/13, w_2 = 16/13\end{aligned}\quad (4.30)$$

Applying these rules on both the element stiffness and mass matrices defines the spectral element (S1) for one-dimensional quadratic interpolation.

For one-dimensional linear elements it is known that a high-order mass, defined as the average of the consistent and the lumped mass results in better accuracy than either regular consistent or lumped mass. For one-dimensional quadratic elements, an average mass matrix, $\mathbf{m}^e = 0.5(\mathbf{m}_c^e + \mathbf{m}_l^e)$, can be obtained by using the quadrature rules,

$$\begin{aligned}\xi_1 = -\xi_3 = -\sqrt{4/5}, \xi_2 = 0 \\ w_1 = w_3 = 5/12, w_2 = 7/6\end{aligned}\quad (4.31)$$

Applying these rules on both the element stiffness and mass matrices defines an alternative Spectral element denoted S2.

The quadrature rules derived for the 1-dimensional quadratic case are extended to two-dimensions by applying these rules in both ξ and η directions. The above rules extended to two dimensions can be summarized as,

Gauss :

$$\begin{aligned}\xi_1 = -\xi_3 = -\sqrt{\frac{3}{5}}, \xi_2 = 0, \\ \eta_1 = -\eta_3 = -\sqrt{\frac{3}{5}}, \eta_2 = 0, \\ w_1 = w_3 = \frac{5}{9}, w_2 = \frac{8}{9}.\end{aligned}\quad (4.33)$$

Lobatto :

$$\begin{aligned}\xi_1 &= -\xi_3 = -1, \xi_2 = 0, \\ \eta_1 &= -\eta_3 = -1, \eta_2 = 0, \\ w_1 &= w_3 = 1/3, w_2 = 4/3.\end{aligned}\tag{4.33}$$

Spectral (S1) :

$$\begin{aligned}\xi_1 &= -\xi_3 = -\sqrt{13/15}, \xi_2 = 0, \\ \eta_1 &= -\eta_3 = -\sqrt{13/15}, \eta_2 = 0, \\ w_1 &= w_3 = 5/13, w_2 = 16/13.\end{aligned}\tag{4.34}$$

Spectral (S2) :

$$\begin{aligned}\xi_1 &= -\xi_3 = -\sqrt{4/5}, \xi_2 = 0, \\ \eta_1 &= -\eta_3 = -\sqrt{4/5}, \eta_2 = 0, \\ w_1 &= w_3 = 5/12, w_2 = 7/6.\end{aligned}\tag{4.35}$$

4.3 Finite Element Formulations for Bi-Quadratic Interpolation

In this section the model problem defined in Chapter 3. is solved using nine-node, bi-quadratic square elements. The finite element approximation within each element can be written as a quadratic interpolation of the nodal degrees of freedom, in natural coordinates,

$$\phi^h(\xi, \eta) = \sum_{i=1}^9 N_i^e(\xi, \eta) d_i^e \tag{4.36}$$

where N_i^e is the shape function of the i th node of element e . The above equation can be written in matrix form as,

$$\phi^h(\xi, \eta) = \mathbf{N}^e \mathbf{d}^e \tag{4.37}$$

where,

$$\mathbf{N}^e = [N_1^e, N_2^e, \dots, N_9^e] \tag{4.38}$$

is the shape function matrix and

$$\mathbf{d}^e = [d_1^e, d_2^e, \dots, d_9^e]^T \quad (4.39)$$

is the element degrees of freedom vector. The bi-quadratic shape functions are defined as tensor product of one-dimensional Lagrange functions,

$$\begin{aligned} N_1 &= L_1(\xi)L_1(\eta) & N_5 &= L_2(\xi)L_1(\eta) & N_2 &= L_3(\xi)L_1(\eta) \\ N_8 &= L_1(\xi)L_2(\eta) & N_9 &= L_2(\xi)L_2(\eta) & N_6 &= L_3(\xi)L_2(\eta) \\ N_4 &= L_1(\xi)L_3(\eta) & N_7 &= L_2(\xi)L_3(\eta) & N_3 &= L_3(\xi)L_3(\eta) \end{aligned} \quad (4.40)$$

where

$$\begin{aligned} L_1(\xi) &= -\xi(1-\xi) \\ L_2(\xi) &= (1-\xi^2) \\ L_3(\xi) &= \frac{\xi(1+\xi)}{2}. \end{aligned} \quad (4.41)$$

Similarly the weighting function can be approximated as,

$$\mathbf{w}^h = \mathbf{N}^e \delta \mathbf{d}^e. \quad (4.42)$$

The gradient,

$$\nabla \phi^h(x, y) = \mathbf{B}^e \mathbf{d}^e \quad (4.43)$$

where

$$\mathbf{B}^e = \mathbf{J}^{-1} \begin{bmatrix} N_{1,\xi} & N_{2,\xi} & \dots & N_{9,\xi} \\ N_{1,\eta} & N_{2,\eta} & \dots & N_{9,\eta} \end{bmatrix}. \quad (4.44)$$

Substituting equations 4.37 and 4.42 into equation 3.15 leads to the element arrays,

$$\mathbf{k}^e = \sum_{a,b=1}^3 \mathbf{B}^{e^T}(\xi_a, \eta_b) \mathbf{B}^e(\xi_a, \eta_b) J^e w_a w_b \quad (4.45)$$

$$\mathbf{m}^e = \sum_{a,b=1}^3 \mathbf{N}^{e^T}(\xi_a, \eta_b) \mathbf{N}^e(\xi_a, \eta_b) J^e w_a w_b \quad (4.46)$$

$$\mathbf{b}^e = \sum_{a=1}^p \mathbf{N}^{e^T}(\xi_a) \mathbf{N}^e(\xi_a) \frac{h^e}{2} w_a \Big|_{\eta=-1}^{\eta=1} + \sum_{b=1}^p \mathbf{N}^{e^T}(\eta_b) \mathbf{N}^e(\eta_b) \frac{h^e}{2} w_b \Big|_{\xi=-1}^{\xi=1} +$$

$$\sum_{a=1}^p \mathbf{N}^{e^T}(\xi_a) \mathbf{N}^e(\xi_a) \frac{h^e}{2} w_a \Big|_{\eta=1} + \sum_{b=1}^p \mathbf{N}^{e^T}(\eta_b) \mathbf{N}^e(\eta_b) \frac{h^e}{2} w_b \Big|_{\xi=-1}$$
(4.47)

$$\mathbf{f}^e = \sum_{a=1}^p \mathbf{N}^{e^T}(\xi_a) g_1 \frac{h^e}{2} w_a \Big|_{\eta=-1}^{\eta=1} + \sum_{b=1}^p \mathbf{N}^{e^T}(\eta_b) g_2 \frac{h^e}{2} w_b \Big|_{\xi=-1}^{\xi=1} +$$

$$\sum_{a=1}^p \mathbf{N}^{e^T}(\xi_a) g_3 \frac{h^e}{2} w_a \Big|_{\eta=1} + \sum_{b=1}^p \mathbf{N}^{e^T}(\eta_b) g_4 \frac{h^e}{2} w_b \Big|_{\xi=-1}$$
(4.48)

where, (ξ_a, η_b) are the quadrature points and (w_a, w_b) are the associated weights. In order to enforce the boundary conditions accurately, the element boundary matrix, \mathbf{b}^e and the element load vector, \mathbf{f}^e , are evaluated using ten point Gauss quadrature rules. For comparison, different quadrature rules are used for stiffness and mass matrices resulting in the following methods,

(a) Galerkin

The element stiffness and mass matrices are evaluated using Gauss quadrature rules resulting in the standard Galerkin method.

(b) Galerkin-Lumped Mass (Galerkin-LM)

The element stiffness matrix is evaluated exactly using Gauss quadrature while the mass matrix is evaluated using Lobatto quadrature rules resulting in the Galerkin method with lumped mass.

(c) Spectral-S1

Both the mass and stiffness matrices are evaluated using spectral quadrature rules, S1.

(d) Spectral-S2

Both the mass and stiffness matrices are evaluated using alternate spectral quadrature rules, S2.

(e) Spectral (S1)-Lumped mass:

The element stiffness matrix is evaluated using spectral (S1) quadrature while the mass matrix is evaluated using lobatto quadrature rules resulting in the spectral (S1) method with lumped mass.

4.4 Galerkin Least Squares Method

The GLS formulation for the model problem was given in equation 3.51. Substituting equation 4.37 into equation 3.51 leads to the modified element dynamic stiffness matrix,

$$\mathbf{s}^e = \mathbf{k}^e - k^2 \mathbf{m}^e + \tilde{\mathbf{k}}^e \quad (4.49)$$

where the additional matrix due to the least-square term is,

$$\begin{aligned} \tilde{\mathbf{k}}^e &= \int_{\Omega^e} \left(\frac{\partial^2 \mathbf{N}^T}{\partial x^2} + \frac{\partial^2 \mathbf{N}^T}{\partial y^2} + k^2 \mathbf{N}^T \right) \left(\frac{\partial^2 \mathbf{N}}{\partial x^2} + \frac{\partial^2 \mathbf{N}}{\partial y^2} + k^2 \mathbf{N} \right) d\Omega \\ &= \int_{-1}^1 \int_{-1}^1 \tau \left(\frac{4}{h^2} \frac{\partial^2 \mathbf{N}^T}{\partial \xi^2} + \frac{4}{h^2} \frac{\partial^2 \mathbf{N}^T}{\partial \eta^2} + k^2 \mathbf{N}^T \right) \\ &\quad \times \left(\frac{4}{h^2} \frac{\partial^2 \mathbf{N}}{\partial \xi^2} + \frac{4}{h^2} \frac{\partial^2 \mathbf{N}}{\partial \eta^2} + k^2 \mathbf{N} \right) \frac{h^2}{4} d\xi d\eta \end{aligned} \quad (4.50)$$

The mesh parameter τ which eliminates dispersion error in one-dimension is, Thompson [1995],

$$\tau k^2 = 1 + \frac{c_1 + \sqrt{c_1^2 - 4c_0c_2}}{2c_2} \quad (4.51)$$

where

$$\begin{aligned} c_0 &= -240(1 - \cos\alpha)\alpha^2 + 8(13 + 2\cos\alpha)\alpha^4 + (\cos\alpha - 3)\alpha^6 \\ c_1 &= -2880(1 - \cos\alpha) + 1440\alpha^2 + 24(\cos\alpha - 6)\alpha^4 + 2(3 - \cos\alpha)\alpha^6 \\ c_2 &= -240(1 - \cos\alpha)\alpha^2 + 40(1 - \cos\alpha)\alpha^2 + (\cos\alpha - 3)\alpha^6 \end{aligned} \quad (4.52)$$

where

$$\alpha = kh. \quad (4.53)$$

4.5 Numerical Results

In this section the accuracy of the two alternate spectral element methods, denoted S1 and S2, are compared to the Galerkin method with consistent, lumped and high-order mass, and with the GLS method. Convergence rates and the pollution effect of these methods are also studied.

Figure 4.3 shows the real component, $\text{Re}(\phi)$, of the solution along the bottom edge Γ_1 . For $kh = 1.5$ corresponding to five quadratic elements per wavelength, both the standard Galerkin and Spectral element method accurately represent the plane-wave solution along mesh diagonals, $\theta = 45^\circ$.

In Figure 4.4, the error over the computational domain Ω , measured in H_1 -semi norm is given. The results show that at a resolution of five elements per wavelength, the error in all the methods is relatively small with the largest error occurring in the Galerkin method along mesh lines, $\theta = 0^\circ$. The two spectral methods S1 and S2 are nearly identical and slightly lower than the GLS error.

In Figure 4.5, the accuracy of the Galerkin method with consistent, lumped and high-order mass are compared to the Spectral element (S1), and to the Spectral element

with lumped mass, Spectral (S1)-LM. The Spectral element has the lowest overall error. However, the error using the Galerkin method is almost the same as the Spectral element. Both Galerkin and Spectral methods with lumped mass exhibit identical error at $\theta = 0^\circ$, as expected, however for wave angles approaching $\theta = 45^\circ$, the Spectral lumped mass element error is significantly lower and is comparable to the Galerkin method with consistent mass.

Figure 4.6 shows the solution profile along Γ_1 when the number of elements per wavelength is decreased from five to three. The error is shown in Figure 4.7. For this coarse mesh the Galerkin method shows significantly larger errors when compared to the Spectral and GLS methods. The accuracy of spectral element (S2) is slightly better than (S1) and GLS.

Figure 4.8 shows large errors for the Galerkin lumped mass element over all wave angles θ . Again, the Galerkin high-order mass and spectral (S1) show comparable accuracy.

Figure 4.9 shows the Spectral (S1) method approaches the convergence rate of the interpolant faster than the Galerkin method, with increase in number of elements, n .

Figures 4.10 shows that as the wavenumber is increased from $k = 30$ to $k = 60$, even as the number of element per wavelength remains constant, the Galerkin error increases substantially, while the Spectral element error remains relatively unchanged.

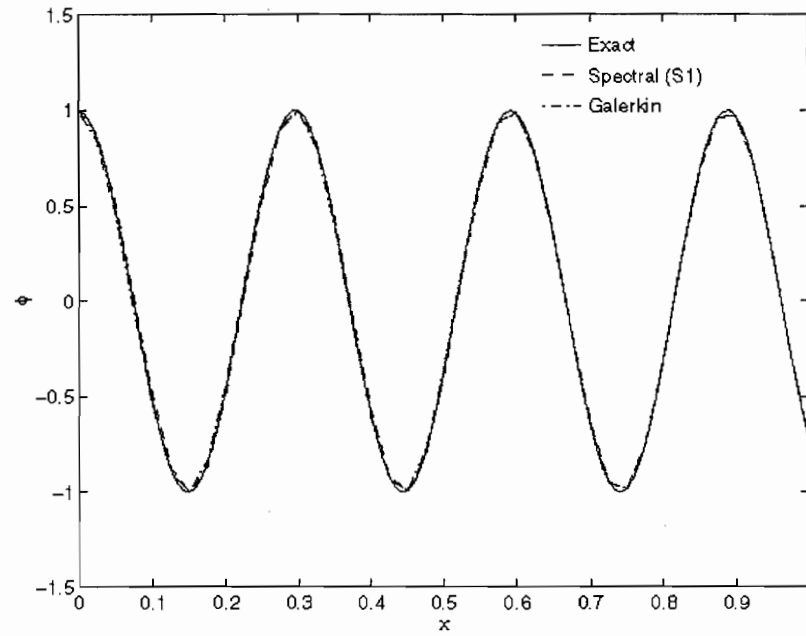


Figure 4.3 Real(ϕ) along the bottom edge, for $k = 30$, $kh = 1.5$, $\theta = 45$.
(5 elements per wave length)

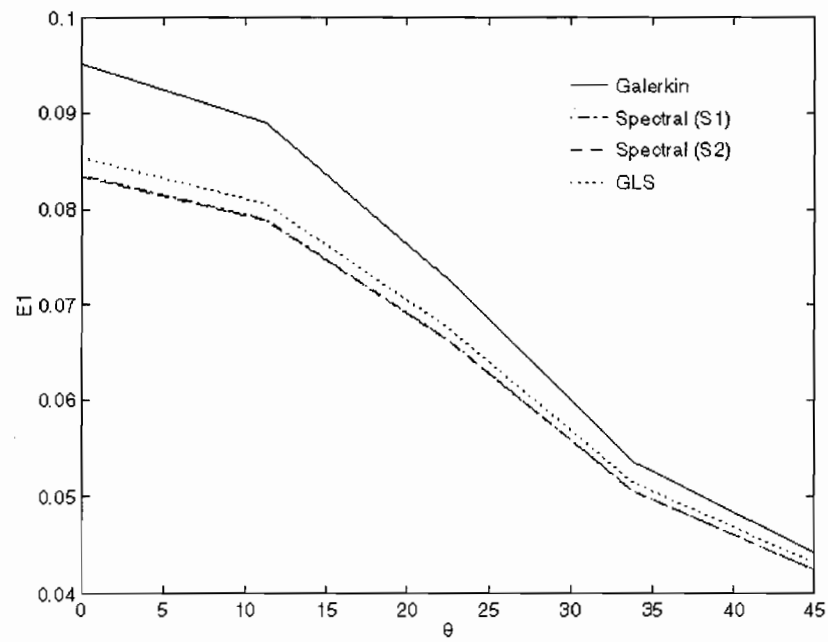


Figure 4.4 Error measured in H_1 -seminorm vs angle in degrees, for $k = 30$, $kh = 1.5$.

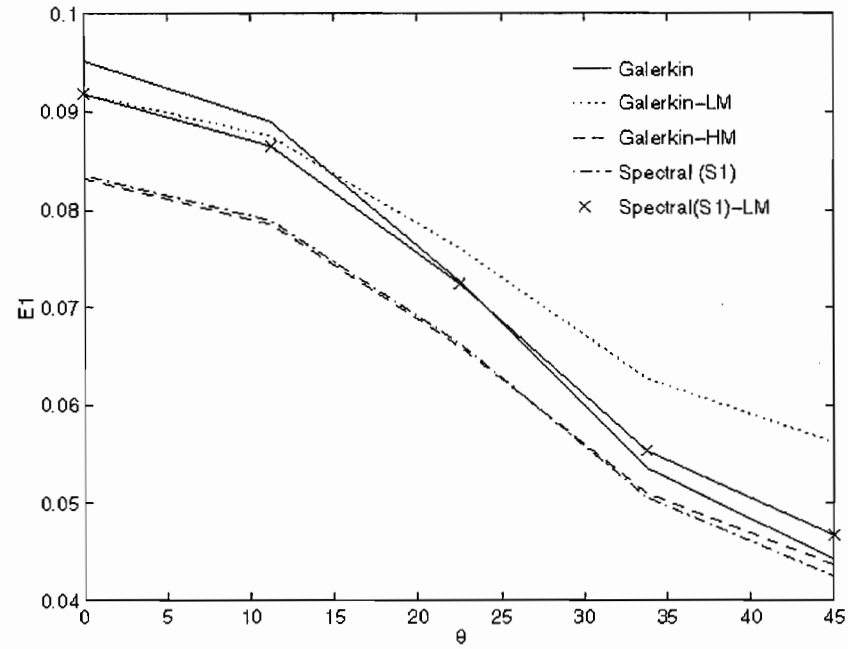


Figure 4.5 Error measured in H_1 -seminorm vs angle in degrees, for $k = 30$, $kh = 1.5$.

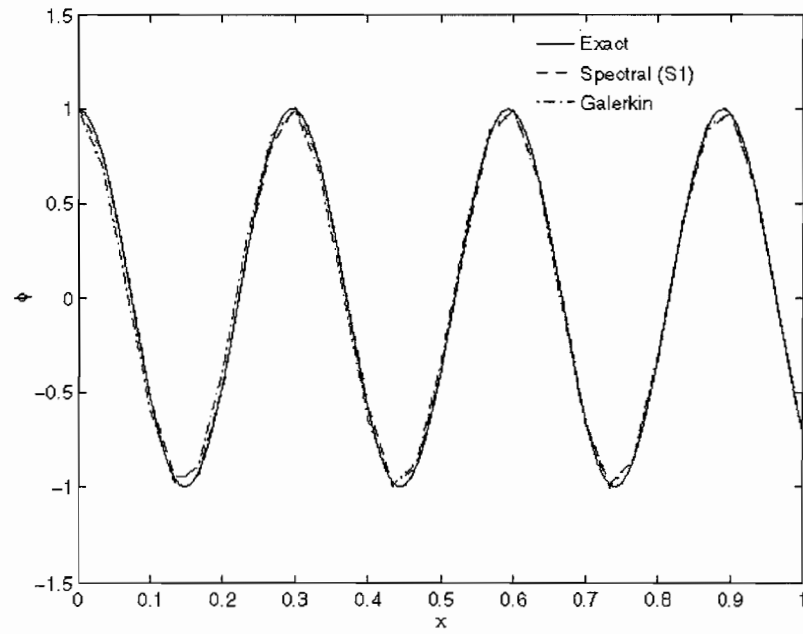


Figure 4.6 $\text{Real}(\phi)$ along the bottom edge, for $k = 30$, $kh = 2$, $\theta = 45$.
(3 elements per wave length)

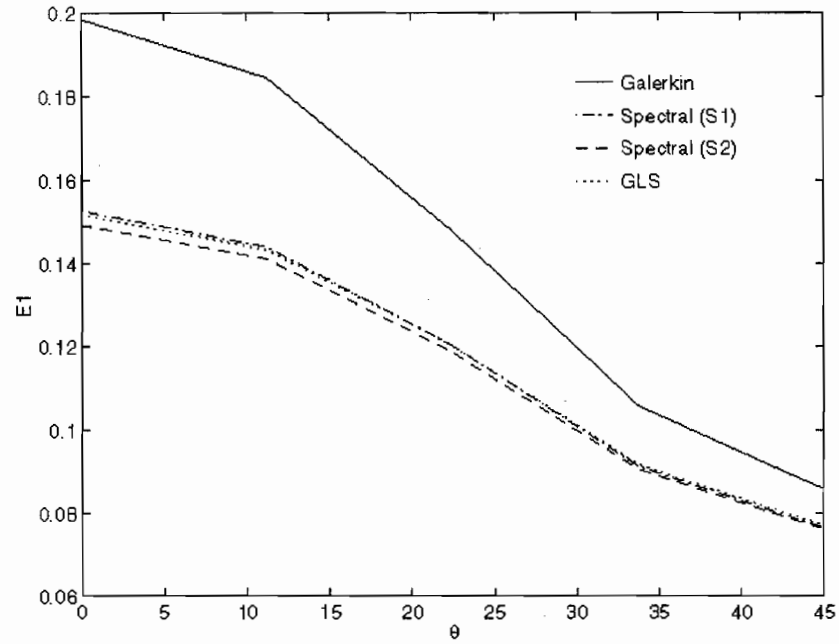


Figure 4.7 Error measured in H_1 -seminorm vs angle in degrees, for $k = 30$, $kh = 2$.

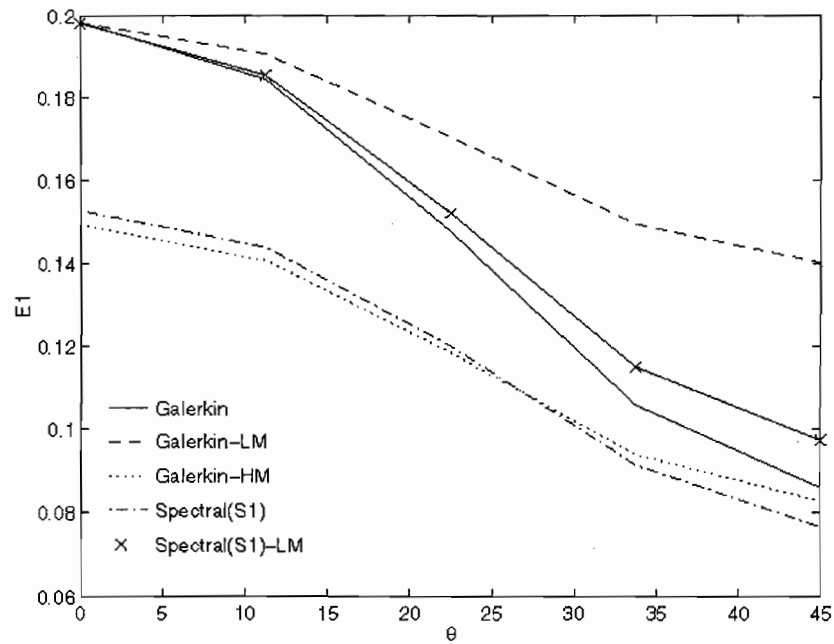


Figure 4.8 Error measured in H_1 -seminorm vs angle in degrees, for $k = 30$, $kh = 2$.

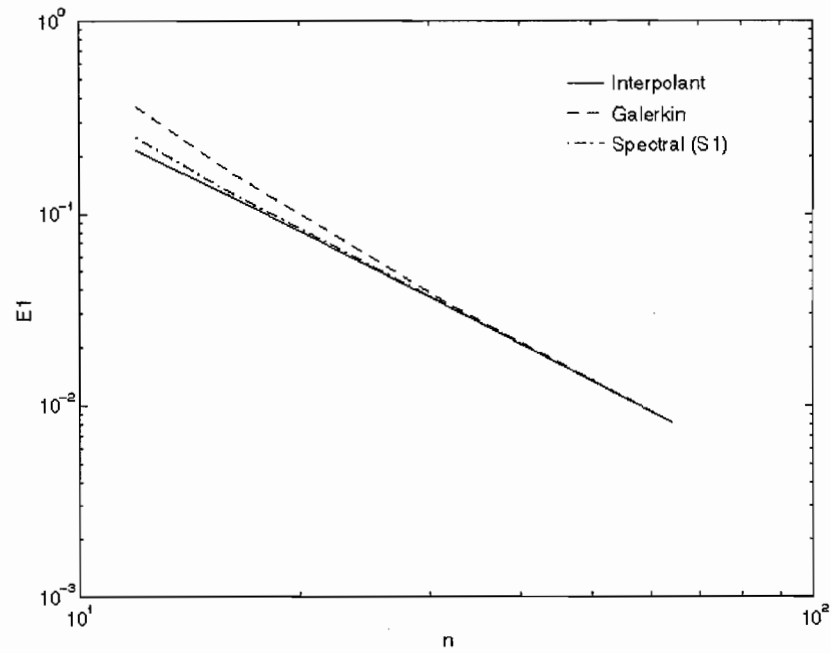


Figure 4.9 Convergence rates (slope = 2) measured in H_1 -seminorm.

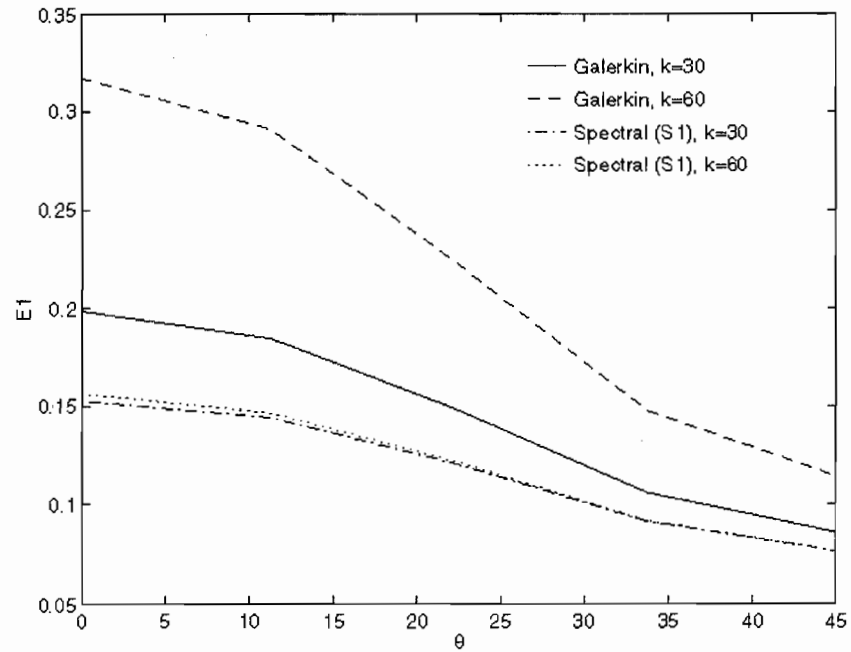


Figure 4.10 Pollution effect for $kh = 2$.

CHAPTER 5

THREE-DIMENSIONAL SPECTRAL ELEMENTS

5.1 Overview

This chapter deals with the design of tri-linear Spectral elements for the three dimensional Helmholtz equation. Dispersion analysis is performed to obtain the characteristic equation, relating the normalized frequency $k = \omega / c$ and the finite element wave vector components, k_1^h, k_2^h, k_3^h . The characteristic equation is then expanded in multi-Taylor's series expansion to determine optimal quadrature rules which result in high-order accuracy. Alternate Galerkin methods including consistent, lumped, and high-order mass are compared.

5.2 Galerkin Finite Element Formulation

In three-dimensions, the Helmholtz equation admits the plane wave solution,

$$\phi(x, y, z) = Ae^{i(k_1 x + k_2 y + k_3 z)} \quad (5.1)$$

where, the wave vector components are,

$$\begin{aligned} k_1 &= k \cos\theta \sin\varphi \\ k_2 &= k \sin\theta \sin\varphi \\ k_3 &= k \cos\varphi \end{aligned} \quad (5.2)$$

and θ is the wave angle in the X-Y plane and φ is the wave angle relative to the z-axis.

Consider a uniform mesh of eight-node tri-linear elements, with element edge length h .

The element domain is parameterized over the tri-unit cube $\bar{\xi} \in (-1,1)^3$ with the usual mapping,

$$\mathbf{x}(\xi, \eta, \zeta) = \sum_{i=1}^8 N_i^e(\xi, \eta, \zeta) x_i^e. \quad (5.3)$$

where x_i^e are nodal coordinates and N_i^e are tri-linear shape functions defined as products of Lagrange interpolation functions,

$$N_i^e(\xi, \eta, \zeta) = \frac{1}{8} (1 + \xi_i \xi) (1 + \eta_i \eta) (1 + \zeta_i \zeta) \quad (5.4)$$

where

$$\mathbf{x} = \begin{bmatrix} x \\ y \\ z \end{bmatrix}, \quad \bar{\xi} = \begin{bmatrix} \xi \\ \eta \\ \zeta \end{bmatrix}. \quad (5.5)$$

On a cube the Jacobian simplifies to

$$J^e = \det \left(\frac{\partial \mathbf{x}}{\partial \bar{\xi}} \right) = \frac{h^3}{8} \quad (5.6)$$

The finite element approximation of ϕ^h and w^h within each element is defined in terms of the nodal degrees of freedom as:

$$\phi^h(\xi, \eta, \zeta) = \sum_{i=1}^9 N_i^e(\xi, \eta, \zeta) d_i^e, \quad (\xi, \eta, \zeta) \in (-1,1)^3 \quad (5.7)$$

and

$$w^h(\xi, \eta, \zeta) = \sum_{i=1}^9 N_i^e(\xi, \eta, \zeta) w_i^e, \quad (\xi, \eta, \zeta) \in (-1,1)^3 \quad (5.8)$$

where, $d_i^e = \phi^h(\xi_i, \eta_i, \zeta_i)$ and $w_i^e = w^h(\xi_i, \eta_i, \zeta_i)$ are the element nodal dof. For dispersion analysis we assume a uniform infinite mesh with homogeneous source $f = 0$.

The (8x8) element dynamic matrix is composed of the stiffness and mass arrays.

$$\mathbf{s}^e = \mathbf{k}^e - k^2 \mathbf{m}^e \quad (5.9)$$

where,

$$\mathbf{k}^e = [k_{ij}^e] \quad (5.10)$$

$$\mathbf{m}^e = [m_{ij}^e] \quad (5.11)$$

and

$$k_{ij}^e = \int_{-1}^1 \int_{-1}^1 \int_{-1}^1 \left(\frac{\partial N_i}{\partial \xi} \frac{\partial N_j}{\partial \xi} + \frac{\partial N_i}{\partial \eta} \frac{\partial N_j}{\partial \eta} + \frac{\partial N_i}{\partial \zeta} \frac{\partial N_j}{\partial \zeta} \right) \frac{1}{J^e} d\xi d\eta d\zeta \quad (5.12)$$

and

$$m_{ij}^e = \int_{-1}^1 \int_{-1}^1 \int_{-1}^1 N_i N_j J^e d\xi d\eta d\zeta. \quad (5.13)$$

The integrals over the tri-unit cube are evaluated using numerical integration.

$$k_{ij}^e = \frac{8}{h^3} \sum_{p=1}^{n_q} \sum_{q=1}^{n_q} \sum_{r=1}^{n_q} \left(\frac{\partial N_i(\xi_p, \eta_q, \zeta_r)}{\partial \xi} \frac{\partial N_j(\xi_p, \eta_q, \zeta_r)}{\partial \xi} + \frac{\partial N_i(\xi_p, \eta_q, \zeta_r)}{\partial \eta} \frac{\partial N_j(\xi_p, \eta_q, \zeta_r)}{\partial \eta} + \frac{\partial N_i(\xi_p, \eta_q, \zeta_r)}{\partial \zeta} \frac{\partial N_j(\xi_p, \eta_q, \zeta_r)}{\partial \zeta} \right) w_p \times w_q \times w_r \quad (5.14)$$

and

$$m_{ij}^e = \frac{h^3}{8} \sum_{a=1}^{n_q} \sum_{b=1}^{n_q} \sum_{c=1}^{n_q} N_i(\xi_a, \eta_b, \zeta_c) N_j(\xi_a, \eta_b, \zeta_c) w_a w_b w_c \quad (5.15)$$

Symmetric quadrature rules are assumed and the number of quadrature points in each

direction $n_q = 2$. Independent quadrature rules are defined for the stiffness matrix,

$$\begin{aligned} w_1 &= w_2 = 1 \\ \xi_1 &= -\xi_2 = x_k \\ \eta_1 &= -\eta_2 = x_k \\ \zeta_1 &= -\zeta_2 = x_k. \end{aligned} \tag{5.16}$$

For the mass matrix,

$$\begin{aligned} w_1 &= w_2 = 1 \\ \xi_1 &= -\xi_2 = x_m \\ \eta_1 &= -\eta_2 = x_m \\ \zeta_1 &= -\zeta_2 = x_m. \end{aligned} \tag{5.17}$$

5.3 Dispersion Relationship

The dispersion relations are obtained by assuming a plain-wave solution propagating at arbitrary angles relative to mesh lines,

$$\phi_{m,n,p} = A^h e^{i(k_1^h hm + k_2^h hm + k_3^h hp)} \tag{5.18}$$

with $i = \sqrt{-1}$. In the above equation, the directional wave vector components are denoted by, $k_1^h = k^h \cos\theta \sin\varphi$, $k_2^h = k^h \sin\theta \sin\varphi$ and $k_3^h = k^h \cos\varphi$, with numerical wave number, $k^h = \sqrt{(k_1^h)^2 + (k_2^h)^2 + (k_3^h)^2}$. Substituting equation 5.18 into 5.9 results in the following dispersion relation,

$$\tilde{S} - k^2 \tilde{M} = 0. \tag{5.19}$$

This equation describes the relationship between the continuous wave number $k = \omega / c$ and the finite element discrete wave vector components k_1^h , k_2^h and k_3^h . In this relation,

\tilde{S} and \tilde{M} represent the transformed stiffness and mass operators respectively, and are defined as,

$$\tilde{S} = \mathbf{1}_y^k \mathbf{1}_z^k \bar{k}_x^2 + \mathbf{1}_x^k \mathbf{1}_z^k \bar{k}_y^2 + \mathbf{1}_x^k \mathbf{1}_y^k \bar{k}_z^2 \quad (5.20)$$

$$\tilde{M} = \mathbf{1}_x^m \mathbf{1}_y^m \mathbf{1}_z^m \quad (5.21)$$

with notation,

$$\bar{k}_x^2 = \frac{2}{h^2}(1 - C_x), \quad \bar{k}_y^2 = \frac{2}{h^2}(1 - C_y) \quad \text{and} \quad \bar{k}_z^2 = \frac{2}{h^2}(1 - C_z) \quad (5.22)$$

$$C_x = \cos(k_x^h h) \quad (5.23)$$

$$C_y = \cos(k_y^h h) \quad (5.24)$$

$$C_z = \cos(k_z^h h) \quad (5.25)$$

$$\mathbf{1}_x^k = 1 - \frac{\epsilon_k}{6}(\bar{k}_x h)^2 \quad (5.26)$$

$$\mathbf{1}_y^k = 1 - \frac{\epsilon_k}{6}(\bar{k}_y h)^2 \quad (5.27)$$

$$\mathbf{1}_z^k = 1 - \frac{\epsilon_k}{6}(\bar{k}_z h)^2 \quad (5.28)$$

$$\mathbf{1}_x^m = 1 - \frac{\epsilon_m}{6}(\bar{k}_x h)^2 \quad (5.29)$$

$$\mathbf{1}_y^m = 1 - \frac{\epsilon_m}{6}(\bar{k}_y h)^2 \quad (5.30)$$

$$\mathbf{1}_z^m = 1 - \frac{\epsilon_m}{6}(\bar{k}_z h)^2. \quad (5.31)$$

Written in another form,

$$k^2 = \tilde{S} / \tilde{M}. \quad (5.32)$$

The exact dispersion relation is,

$$k^2 = \left(\frac{\omega}{c} \right)^2 = (k_1^2 + k_2^2 + k_3^2). \quad (5.33)$$

5.4 Selection of Quadrature Parameters

In this section optimal values are chosen for the quadrature parameters ε_k and ε_m based on Taylor's series expansion. These values result in quadrature rules which give high-order accurate Spectral elements. Other quadrature rules for ε_k and ε_m and their accuracies are compared.

Expanding the characteristic equation 5.32 in multi-Taylor's series expansion of k_1^h , k_2^h and k_3^h yields,

$$\begin{aligned} k^2 = & (k^h)^2 + \left[\left(-\frac{1}{12}\right)h^2 + \left(\frac{1}{6}\right)h^2 \varepsilon_m \right] (k_1^h)^4 + \left[\left(-\frac{1}{3}\right)\varepsilon_k h^2 + \left(\frac{1}{3}\right)\varepsilon_m h^2 \right] \\ & (k_1^h)^2 (k_2^h)^2 + \left[\left(-\frac{1}{3}\right)\varepsilon_k h^2 + \left(\frac{1}{3}\right)\varepsilon_m h^2 \right] (k_1^h)^2 (k_3^h)^2 + \\ & \left[\left(-\frac{1}{12}\right)h^2 + \left(\frac{1}{6}\right)h^2 \varepsilon_m \right] (k_2^h)^4 + \left[\left(-\frac{1}{3}\right)\varepsilon_k h^2 + \left(\frac{1}{3}\right)\varepsilon_m h^2 \right] (k_2^h)^2 (k_3^h)^2 \\ & \left[\left(-\frac{1}{12}\right)h^2 + \left(\frac{1}{6}\right)h^2 \varepsilon_m \right] (k_3^h)^4 + \dots \end{aligned} \quad (5.34)$$

Comparing with the exact relation we observe that quadrature corresponding to,

$$\varepsilon = \varepsilon_k = \varepsilon_m = 1/2 \quad (5.35)$$

annihilates the fourth-order terms, leaving an error of sixth-order only.

The quadrature rules with the above conditions are,

$$\begin{aligned}
 \xi_1 &= -\xi_2 = \sqrt{2/3} \\
 \eta_1 &= -\eta_2 = \sqrt{2/3} \\
 \zeta_1 &= -\zeta_2 = \sqrt{2/3} \\
 w_1 &= w_2 = 1
 \end{aligned}
 \tag{5.36}$$

and applying the above rules on both the stiffness and the mass terms yields the high-order accurate eight-node tri-linear Spectral elements.

The following table summarizes several values of ϵ_k and ϵ_m , the resulting Taylor's series expansion, the corresponding methods and their accuracies.

Table 5.1

3-D Quadrature Parameters and Corresponding Methods

Quadrature Parameters	Taylor's Series Expansion	Method
	$E_k = k^2 - (k^h)^2$	
$\varepsilon_k = 0, \varepsilon_m = 0$	$-\frac{h^2}{12}((k_1^h)^4 + (k_2^h)^4 + (k_3^h)^4)$	Central Difference Method
$\varepsilon_k = 1, \varepsilon_m = 1$	$+\frac{h^2}{12}((k_1^h)^4 + (k_2^h)^4 + (k_3^h)^4)$	Galerkin, Consistent Mass
$\varepsilon_k = 1, \varepsilon_m = 0$	$-\frac{h^2}{12}((k_1^h)^4 + (k_2^h)^4 + (k_3^h)^4)$ $+4(k_1^h)^2(k_2^h)^2 + 4(k_1^h)^2(k_3^h)^2$ $+4(k_2^h)^2(k_3^h)^2)$	Galerkin, Diagonal Mass
$\varepsilon_k = 1, \varepsilon_m = 1/2$	$-\frac{h^2}{12}(2(k_1^h)^2(k_2^h)^2$ $+2(k_2^h)^2(k_3^h)^2 + 2(k_1^h)^2(k_3^h)^2)$	Galerkin, Higher-Order Mass
$\varepsilon_k = 1/2, \varepsilon_m = 1/2$	$-\frac{h^2}{240}((k_1^h)^6 + (k_2^h)^6 + (k_3^h)^6)$	Spectral
$\varepsilon_k = 1/2, \varepsilon_m = 0$	$-\frac{h^2}{12}(k^h)^4$	Spectral, Diagonal Mass

5.5 Model Problem

5.5.1 Strong form of the Boundary Value Problem (BVP)

Consider a BVP for plane wave propagation on a tri-unit cubic domain, see Figure

5.1. The objective is to find $\phi(x, y, z)$, the spatial component of the acoustic pressure such that the Helmholtz equation is satisfied:

$$\nabla^2 \phi + k^2 \phi = 0 \quad \text{in } \Omega := (0,1) \times (0,1) \times (0,1) \quad (5.37)$$

with non-reflecting boundary conditions,

$$ik\phi + \frac{\partial \phi}{\partial n} = g \quad \text{on } \Gamma_s \text{ for } s \in \{1,2,3,4,5,6\}. \quad (5.38)$$

In the above, $k = \omega / c$ is the wave number, $i = \sqrt{-1}$, $\partial / \partial n$ is the normal derivative on Γ_s . The function g depends on k, θ, φ :

$$\begin{aligned} g(\mathbf{x}) &= g_1(x, z) & \text{for } \mathbf{x} \in \Gamma_1 &:= (0,0,0) \times (1,0,0) \times (1,0,1) \times (0,0,1) \\ &= g_2(y, z) & \text{for } \mathbf{x} \in \Gamma_2 &:= (1,0,0) \times (1,1,0) \times (1,1,1) \times (1,0,1) \\ &= g_3(x, z) & \text{for } \mathbf{x} \in \Gamma_3 &:= (1,1,0) \times (0,1,0) \times (0,1,1) \times (1,1,1) \\ &= g_4(y, z) & \text{for } \mathbf{x} \in \Gamma_4 &:= (0,1,0) \times (0,0,0) \times (0,0,1) \times (0,1,1) \\ &= g_5(x, y) & \text{for } \mathbf{x} \in \Gamma_5 &:= (0,0,0) \times (1,0,0) \times (1,1,0) \times (0,1,0) \\ &= g_6(x, y) & \text{for } \mathbf{x} \in \Gamma_6 &:= (0,0,1) \times (1,0,1) \times (1,1,1) \times (0,1,1) \end{aligned} \quad (5.39)$$

where

$$\begin{aligned} g_1(x, z) &= i(k - k_2)e^{i(k_1x + k_3z)} \\ g_2(y, z) &= i(k + k_1)e^{i(k_1 + k_2y + k_3z)} \\ g_3(x, z) &= i(k + k_2)e^{i(k_1x + k_2 + k_3z)} \\ g_4(y, z) &= i(k - k_1)e^{i(k_2y + k_3z)} \\ g_5(x, y) &= i(k - k_3)e^{i(k_1x + k_2y)} \\ g_6(x, y) &= i(k + k_3)e^{i(k_1x + k_2y + k_3)} \end{aligned} \quad (5.40)$$

and

$$k_1 = k \cos \theta \sin \varphi, \quad k_2 = k \sin \theta \sin \varphi, \quad k_3 = k \cos \varphi. \quad (5.41)$$

The boundary condition, equation 5.38, is designed so that the exact solution to the BVP is the plane-wave solution, $\phi(x, y, z) = e^{i(k_1 x + k_2 y + k_3 z)}$.

5.5.2 Weak form of the BVP

The weak form of the BVP can be obtained formally by multiplying equation 5.37 with the complex conjugate of a weighting function. Then, after integration by parts and substitution of the natural boundary conditions, equation 5.38 and 5.39, the variational problem can be defined as: Find ϕ such that for all w ,

$$A(w, \phi) = L(w) \quad (5.42)$$

where,

$$A(w, \phi) = \int_{\Omega} \nabla w \bullet \nabla \phi \, d\Omega - k^2 \int_{\Omega} w \phi \, d\Omega + ik \int_{\Gamma} w \phi \, d\Gamma \quad (5.43)$$

and

$$L(w) = \int_{\Gamma} w g \, d\Gamma = \sum_{s=1}^6 \int_{\Gamma_s} w_s g_s \, d\Gamma \quad (5.44)$$

The bi-linear operator A, involves a complex number term on the boundary Γ due to the form of equation 5.38. The linear operator L, also is complex due to the definition of g.

5.5.3 Galerkin Form of the BVP

The Galerkin form of the BVP is simply a re-statement of the weak form with the solution function $\phi(x, y, z)$ replaced by an approximate solution $\phi^h(x, y, z)$, and the

weighting function $w(x, y, z)$ replaced by an approximate weighting function $w^h(x, y, z)$, i.e.

$$\begin{aligned}\phi(x, y, z) &\approx \phi^h(x, y, z) \\ w(x, y, z) &\approx w^h(x, y, z).\end{aligned}\tag{5.45}$$

The superscript h is used to indicate that the quantity is an approximation. Making these substitutions the Galerkin form of the BVP can be defined as: Find $\phi^h(x, y, z)$, such that for all $w^h(x, y, z)$,

$$A(w^h, \phi^h) = L(w^h)\tag{5.46}$$

where

$$A(w^h, \phi^h) = \int_{\Omega} \nabla w^h \bullet \nabla \phi^h d\Omega - k^2 \int_{\Omega} w^h \phi^h d\Omega + ik \int_{\Gamma} w^h \phi^h d\Gamma\tag{5.47}$$

$$L(w^h) = \int_{\Gamma} w^h g^h d\Gamma\tag{5.48}$$

5.5.4 Finite Element Formulation

The finite element analysis of the above model problem was performed using a mesh of eight-node tri-linear cube elements. The domain is discretized into n finite elements as shown in Figure 5.2. The elements are arbitrarily numbered from bottom left corner starting at 1 and running to n to the top right corner. Consider a typical element e , such that $1 \leq e \leq n$, and let the interval covered by the element e be denoted by Ω^e such that,

$$\Omega = \Omega^1 \cup \Omega^2 \cup \dots \cup \Omega^e \cup \dots \cup \Omega^n.\tag{5.49}$$

After discretization the Galerkin equation can be written as,

$$\begin{aligned} \sum_{e=1}^n \left[\int_{\Omega^e} \nabla w^h \bullet \nabla \phi^h d\Omega^e - k^2 \int_{\Omega^e} w^h \phi^h d\Omega^e + ik \int_{\Gamma_s^e} w^h \phi^h d\Gamma_s^e \right] \\ = \sum_{e=1}^n \int_{\Gamma_s^e} w^h \phi^h d\Gamma_s^e \end{aligned} \quad (5.50)$$

The finite element approximation within each element can be written as an interpolation of the nodal degrees of freedom,

$$\phi^h = \sum_{i=1}^l N_i^e d_i^e \quad (5.51)$$

where N_i^e is the shape function of the i^{th} node of element e and l is the number of degrees of freedom per element. For a eight node element, $l = 8$, equation 5.51 can be written in matrix form as,

$$\phi^h = \mathbf{N}^e \mathbf{d}^e \quad (5.52)$$

where

$$\mathbf{N}^e = [N_1^e, N_2^e, \dots, N_8^e] \quad (5.53)$$

is the shape function array, where the shape functions N_i^e are standard tri-linear Lagrange functions defined as,

$$\begin{aligned} N_1^e &= \frac{1}{8}(1-\xi)(1-\eta)(1-\zeta), & N_2^e &= \frac{1}{8}(1+\xi)(1-\eta)(1-\zeta), \\ N_3^e &= \frac{1}{8}(1+\xi)(1+\eta)(1-\zeta), & N_4^e &= \frac{1}{8}(1-\xi)(1+\eta)(1-\zeta), \\ N_5^e &= \frac{1}{8}(1-\xi)(1-\eta)(1+\zeta), & N_6^e &= \frac{1}{8}(1+\xi)(1-\eta)(1+\zeta), \\ N_7^e &= \frac{1}{8}(1+\xi)(1+\eta)(1+\zeta), & N_8^e &= \frac{1}{8}(1-\xi)(1+\eta)(1+\zeta). \end{aligned} \quad (5.54)$$

and

$$\mathbf{d}^e = [d_1^e, d_2^e, \dots, d_8^e]^T \quad (5.55)$$

is the element degrees of freedom vector. Similarly the weighting function can be written as,

$$w^h = \mathbf{N}^e \delta \mathbf{d}^e. \quad (5.56)$$

Using the above approximations, the gradient can be written as,

$$\nabla \phi^h = \begin{bmatrix} \frac{\partial \phi^h}{\partial x} \\ \frac{\partial \phi^h}{\partial y} \\ \frac{\partial \phi^h}{\partial z} \end{bmatrix} = \mathbf{B}^e \mathbf{d}^e \quad (5.57)$$

where

$$\mathbf{B}^e = \begin{bmatrix} N_{1,x}^e, N_{2,x}^e, \dots, N_{8,x}^e \\ N_{1,y}^e, N_{2,y}^e, \dots, N_{8,y}^e \\ N_{1,z}^e, N_{2,z}^e, \dots, N_{8,z}^e \end{bmatrix}. \quad (5.58)$$

Similarly the gradient of the weighting function can be written as,

$$\nabla w^h = \mathbf{B}^e \delta \mathbf{d}^e. \quad (5.59)$$

Substituting the finite element approximation, equation 5.52 into equation 5.50 gives,

$$\begin{aligned} \sum_{e=1}^n \delta \mathbf{d}^{eT} \left\{ \int_{\Omega^e} \mathbf{B}^{eT} \mathbf{B}^e d\Omega^e - k^2 \int_{\Omega^e} \mathbf{N}^{eT} \mathbf{N}^e d\Omega^e + ik \int_{\Gamma^e} \mathbf{N}^{eT} \mathbf{N}^e d\Gamma^e \right\} \mathbf{d}^e \\ = \sum_{e=1}^n \delta \mathbf{d}^{eT} \left\{ \int_{\Gamma^e} \mathbf{N}^{eT} g d\Gamma^e \right\}. \end{aligned} \quad (5.60)$$

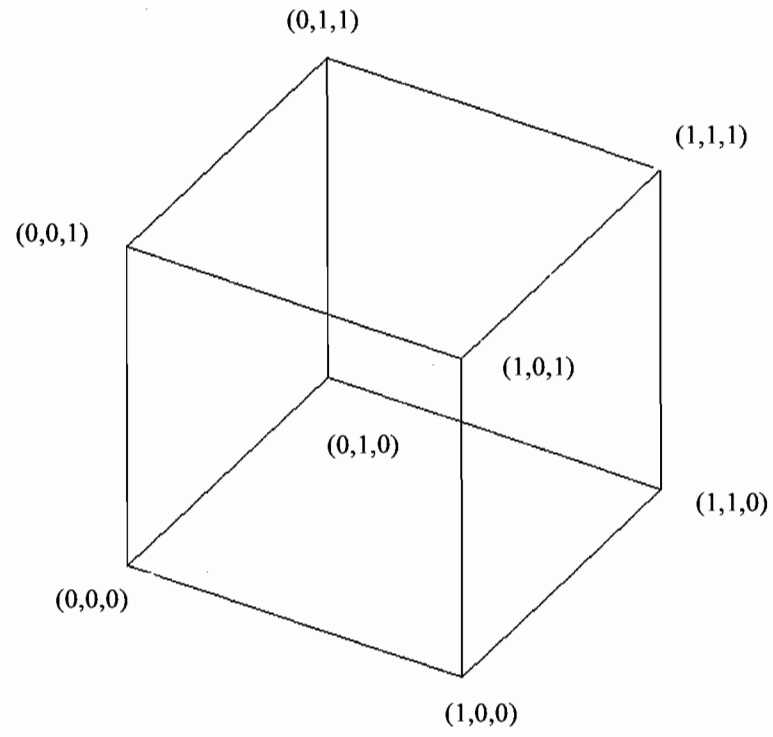


Figure 5.1 3-D Model Problem

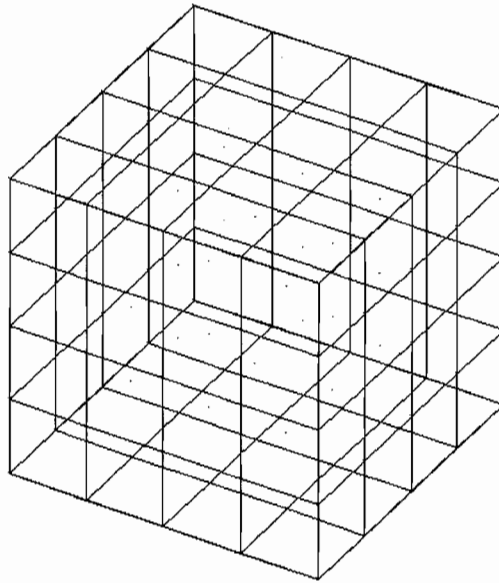


Figure 5.2 Tri-Linear Finite element mesh.

Defining the element matrices,

$$\mathbf{k}^e = \int_{\Omega^e} \mathbf{B}^{eT} \mathbf{B}^e d\Omega^e \quad (\text{element stiffness matrix}) \quad (5.61)$$

$$\mathbf{m}^e = \int_{\Omega^e} \mathbf{N}^{eT} \mathbf{N}^e d\Omega^e \quad (\text{element mass matrix}) \quad (5.62)$$

$$\mathbf{b}^e = \int_{\Gamma^e} \mathbf{N}^{eT} \mathbf{N}^e d\Gamma^e \quad (\text{element boundary condition matrix}) \quad (5.63)$$

$$\mathbf{f}^e = \int_{\Gamma^e} \mathbf{N}^{eT} g d\Gamma^e \quad (\text{element load vector}). \quad (5.64)$$

equation 5.60 may be written as,

$$\sum_{e=1}^n \delta \mathbf{d}^{eT} \{ \mathbf{k}^e - k^2 \mathbf{m}^e + ik \mathbf{b}^e \} \mathbf{d}^e = \sum_{e=1}^n \delta \mathbf{d}^{eT} \mathbf{f}^e. \quad (5.65)$$

Relating the local degrees of freedom to global degrees of freedom and assembly leads to the global matrix problem,

$$(\mathbf{K} - k^2 \mathbf{M} + ik \mathbf{B}) \mathbf{d} = \mathbf{F}. \quad (5.66)$$

For numerical quadrature, the element coordinates are parameterized by natural coordinates, $-1 \leq \xi \leq 1, -1 \leq \eta \leq 1, -1 \leq \zeta \leq 1$. For the eight-node element the corner node points defined in natural coordinates are,

$$\begin{aligned} (\xi_1, \eta_1) &= (-1, -1, 1), & (\xi_2, \eta_2) &= (1, -1, 1), \\ (\xi_3, \eta_3) &= (1, -1, -1), & (\xi_4, \eta_4) &= (-1, -1, -1), \\ (\xi_5, \eta_5) &= (-1, 1, 1), & (\xi_6, \eta_6) &= (1, 1, 1), \\ (\xi_7, \eta_7) &= (1, 1, -1), & (\xi_8, \eta_8) &= (-1, 1, -1). \end{aligned} \quad (5.67)$$

The global coordinates (x, y, z) are related to the element natural coordinates (ξ, η, ζ) by,

$$\begin{aligned} x(\xi, \eta, \zeta) &= \sum_{i=1}^4 N_i^e(\xi, \eta, \zeta) x_i^e, \\ y(\xi, \eta, \zeta) &= \sum_{i=1}^4 N_i^e(\xi, \eta, \zeta) y_i^e, \\ z(\xi, \eta, \zeta) &= \sum_{i=1}^4 N_i^e(\xi, \eta, \zeta) z_i^e. \end{aligned} \quad (5.68)$$

The relation between physical and natural derivatives is given by,

$$\begin{bmatrix} \frac{\partial N_i}{\partial x} \\ \frac{\partial N_i}{\partial y} \\ \frac{\partial N_i}{\partial z} \end{bmatrix} = \mathbf{J}^{-1} \begin{bmatrix} \frac{\partial N_i}{\partial \xi} \\ \frac{\partial N_i}{\partial \eta} \\ \frac{\partial N_i}{\partial \zeta} \end{bmatrix} \quad (5.69)$$

where

$$\mathbf{J} = \begin{bmatrix} \frac{\partial x}{\partial \xi} & \frac{\partial y}{\partial \xi} & \frac{\partial z}{\partial \xi} \\ \frac{\partial x}{\partial \eta} & \frac{\partial y}{\partial \eta} & \frac{\partial z}{\partial \eta} \\ \frac{\partial x}{\partial \zeta} & \frac{\partial y}{\partial \zeta} & \frac{\partial z}{\partial \zeta} \end{bmatrix} \quad (5.70)$$

is the Jacobian matrix. For cube element with edge length h^e , the Jacobian matrix simplifies to,

$$\mathbf{J} = \begin{bmatrix} \frac{h^e}{2} & 0 & 0 \\ 0 & \frac{h^e}{2} & 0 \\ 0 & 0 & \frac{h^e}{2} \end{bmatrix} \quad (5.71)$$

resulting in a constant determinant,

$$J^e = \det(\mathbf{J}) = \frac{(h^e)^3}{8}. \quad (5.72)$$

Based on this mapping equation 5.58 may be written in natural coordinates as,

$$\mathbf{B}^e = \mathbf{J}^{-1} \begin{bmatrix} N_{1,\xi}, N_{2,\xi}, \dots, N_{8,\xi} \\ N_{1,\eta}, N_{2,\eta}, \dots, N_{8,\eta} \\ N_{1,\zeta}, N_{2,\zeta}, \dots, N_{8,\zeta} \end{bmatrix}. \quad (5.73)$$

Using a change of variable,

$$\int_{\Omega^e} f(x, y, z) dx dy dz = \int_{-1}^1 \int_{-1}^1 \int_{-1}^1 f(\xi, \eta, \zeta) J^e d\xi d\eta d\zeta \quad (5.74)$$

the element matrices in natural coordinates are,

$$\mathbf{k}^e = \int_{-1}^1 \int_{-1}^1 \int_{-1}^1 \mathbf{B}^{eT} \mathbf{B}^e J^e d\xi d\eta d\zeta \quad (5.74)$$

$$\mathbf{m}^e = \int_{-1}^1 \int_{-1}^1 \int_{-1}^1 \mathbf{N}^{eT} \mathbf{N}^e J^e d\xi d\eta d\zeta \quad (5.75)$$

$$\begin{aligned} \mathbf{b}^e = & \left(\int_{-1}^1 \int_{-1}^1 \mathbf{N}^{eT} \mathbf{N}^e \frac{(h^e)^2}{4} d\xi d\zeta \right)_{\eta=-1} + \left(\int_{-1}^1 \int_{-1}^1 \mathbf{N}^{eT} \mathbf{N}^e \frac{(h^e)^2}{4} d\eta d\zeta \right)_{\xi=1} \\ & + \left(\int_{-1}^1 \int_{-1}^1 \mathbf{N}^{eT} \mathbf{N}^e \frac{(h^e)^2}{4} d\xi d\zeta \right)_{\eta=1} + \left(\int_{-1}^1 \int_{-1}^1 \mathbf{N}^{eT} \mathbf{N}^e \frac{(h^e)^2}{4} d\eta d\zeta \right)_{\xi=-1} \\ & + \left(\int_{-1}^1 \int_{-1}^1 \mathbf{N}^{eT} \mathbf{N}^e \frac{(h^e)^2}{4} d\xi d\eta \right)_{\zeta=-1} + \left(\int_{-1}^1 \int_{-1}^1 \mathbf{N}^{eT} \mathbf{N}^e \frac{(h^e)^2}{4} d\xi d\eta \right)_{\zeta=1} \end{aligned} \quad (5.76)$$

$$\begin{aligned} \mathbf{f}^e = & \left(\int_{-1}^1 \int_{-1}^1 \mathbf{N}^{eT} g_1 \frac{(h^e)^2}{4} d\xi d\zeta \right)_{\eta=-1} + \left(\int_{-1}^1 \int_{-1}^1 \mathbf{N}^{eT} g_2 \frac{(h^e)^2}{4} d\eta d\zeta \right)_{\xi=1} \\ & + \left(\int_{-1}^1 \int_{-1}^1 \mathbf{N}^{eT} g_3 \frac{(h^e)^2}{4} d\xi d\zeta \right)_{\eta=1} + \left(\int_{-1}^1 \int_{-1}^1 \mathbf{N}^{eT} g_4 \frac{(h^e)^2}{4} d\eta d\zeta \right)_{\xi=-1} \\ & + \left(\int_{-1}^1 \int_{-1}^1 \mathbf{N}^{eT} g_5 \frac{(h^e)^2}{4} d\xi d\eta \right)_{\zeta=1} + \left(\int_{-1}^1 \int_{-1}^1 \mathbf{N}^{eT} g_6 \frac{(h^e)^2}{4} d\xi d\eta \right)_{\zeta=-1}. \end{aligned} \quad (5.77)$$

The arrays are evaluated using numerical quadrature,

$$\mathbf{k}^e = \sum_{a,b,c=1}^2 \mathbf{B}^{e^T}(\xi_a, \eta_b, \zeta_c) \mathbf{B}^e(\xi_a, \eta_b, \zeta_c) J^e w_a w_b w_c \quad (5.78)$$

$$\mathbf{m}^e = \sum_{a,b,c=1}^2 \mathbf{N}^{e^T}(\xi_a, \eta_b, \zeta_c) \mathbf{N}^e(\xi_a, \eta_b, \zeta_c) J^e w_a w_b w_c \quad (5.79)$$

$$\begin{aligned} \mathbf{b}^e = & \sum_{a,c=1}^p \mathbf{N}^{e^T}(\xi_a, \zeta_c) \mathbf{N}^e(\xi_a, \zeta_c) \frac{(h^e)^2}{4} w_a w_c \Big|_{\eta=-1} \\ & + \sum_{b,c=1}^p \mathbf{N}^{e^T}(\eta_b, \zeta_c) \mathbf{N}^e(\eta_b, \zeta_c) \frac{(h^e)^2}{4} w_b w_c \Big|_{\xi=1} \\ & + \sum_{a,c=1}^p \mathbf{N}^{e^T}(\xi_a, \zeta_c) \mathbf{N}^e(\xi_a, \zeta_c) \frac{(h^e)^2}{4} w_a w_c \Big|_{\eta=1} \\ & + \sum_{b,c=1}^p \mathbf{N}^{e^T}(\eta_b, \zeta_c) \mathbf{N}^e(\eta_b, \zeta_c) \frac{(h^e)^2}{4} w_b w_c \Big|_{\xi=-1} \\ & + \sum_{a,b=1}^p \mathbf{N}^{e^T}(\xi_a, \eta_b) \mathbf{N}^e(\xi_a, \eta_b) \frac{(h^e)^2}{4} w_a w_b \Big|_{\zeta=-1} \\ & + \sum_{a,b=1}^p \mathbf{N}^{e^T}(\xi_a, \eta_b) \mathbf{N}^e(\xi_a, \eta_b) \frac{(h^e)^2}{4} w_a w_b \Big|_{\zeta=1} \end{aligned} \quad (5.80)$$

$$\begin{aligned} \mathbf{f}^e = & \sum_{a,c=1}^p \mathbf{N}^{e^T}(\xi_a, \zeta_c) g_1 \frac{(h^e)^2}{4} w_a w_c \Big|_{\eta=-1} \\ & + \sum_{b,c=1}^p \mathbf{N}^{e^T}(\eta_b, \zeta_c) g_2 \frac{(h^e)^2}{4} w_b w_c \Big|_{\xi=1} \\ & + \sum_{a,c=1}^p \mathbf{N}^{e^T}(\xi_a, \zeta_c) g_3 \frac{(h^e)^2}{4} w_a w_c \Big|_{\eta=1} \\ & + \sum_{b,c=1}^p \mathbf{N}^{e^T}(\eta_b, \zeta_c) g_4 \frac{(h^e)^2}{4} w_b w_c \Big|_{\xi=-1} \\ & + \sum_{a,b=1}^p \mathbf{N}^{e^T}(\xi_a, \eta_b) g_5 \frac{(h^e)^2}{4} w_a w_b \Big|_{\zeta=-1} \\ & + \sum_{a,b=1}^p \mathbf{N}^{e^T}(\xi_a, \eta_b) g_6 \frac{(h^e)^2}{4} w_a w_b \Big|_{\zeta=1} \end{aligned} \quad (5.81)$$

where, (ξ_a, η_b, ζ_c) are the quadrature points and (w_a, w_b, w_c) are the weights. In order to enforce the boundary conditions accurately, the element boundary matrix \mathbf{b}^e and the element load vector \mathbf{f}^e are evaluated using ten point Gauss quadrature ($p = 10$). For the element mass and stiffness matrices two point Gauss and Spectral quadrature rules are used.

5.5 Preliminary Results

Figure 5.3 shows the real component of the solution along the bottom edge Γ_1 for $\theta = 45^\circ$, $\phi = 0^\circ$, representing wave propagation in X-Y plane, and five elements per wavelength. For $kh = 1.5$, (20x20x20) elements were used. It can be seen that for the same number of elements per wavelength the Galerkin method using Gauss quadrature on both stiffness and mass shows a larger phase error when compared to the Spectral element. These results are similar to the two-dimensional model problem for waves propagating along the diagonal.

To obtain greater accuracy more than five elements per wavelength are needed which would increase the total number of elements, greater than 8000, approaching the effective limit of MATLAB memory capabilities due to which further numerical studies on the three-dimensional model problem couldn't be performed. In order to solve larger systems with greater degrees of freedom, programming languages like C, FORTRAN, with efficient memory storage capabilities should be used. The study of the performance of tri-linear spectral studies in comparison to other competing methods is suggested as future work..

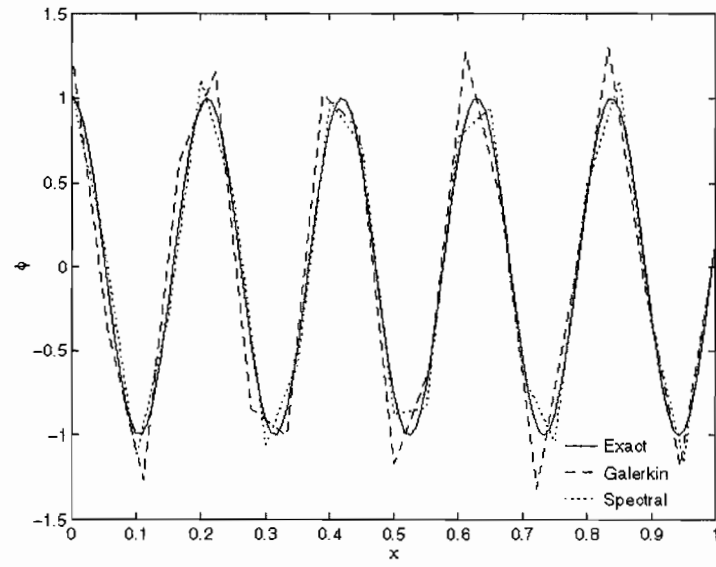


Figure5.3 Real(ϕ) along the bottom edge, for $k = 30$, $kh = 1.5$, $\theta = 45^\circ$, $\varphi = 0^\circ$.
(five elements per wavelength)

CHAPTER 6

CONCLUSIONS AND FUTURE WORK

6.1 Conclusions

In this work a high-order accurate spectral element method was developed that can be used directly both in the frequency domain to approximate the Helmholtz equation and in the time domain to approximate the wave equation. The high-order spectral method employs numerical quadrature points which lead to reduced numerical dispersion. To study the accuracy of several competing methods, we considered the two-dimensional wave equation (Helmholtz equation) on a bi-unit square domain. On the four edges of the square non-reflecting boundary conditions were prescribed which allow plane wave solutions to be developed at different orientations with respect to mesh lines. Finite element analysis of this model problem was performed using elements with both bi-linear and bi-quadratic interpolations. The accuracy of standard Galerkin method, Galerkin least squares, Generalized finite element method and high-order Spectral elements as a function of wavenumber and element size were compared. The accuracy of the high-order spectral elements was significantly improved when compared to the Galerkin method both for linear and quadratic elements. It was also confirmed that for the Galerkin method and a fixed number of elements per wavelength, the accuracy decreases with increasing wavenumber while this pollution effect was negligible for the spectral element. Finally, the high-order quadrature points were extended to three-dimensions, resulting in 3D spectral elements with reduced dispersion error.

Major results from this study include:

1. Optimal quadrature rules were determined which reduces both dispersion and pollution error for four-node bi-linear elements. The use of these rules gives no increase in computational expense over standard Gauss quadrature.
2. Numerical results for plane waves oriented at different angles relative to mesh lines demonstrated the improved accuracy of the spectral element using optimal quadrature rules over the standard Galerkin method.
3. A lumped mass version of the spectral element was derived which is more accurate than Galerkin lumped mass element. The accuracy of this spectral lumped mass element is relatively independent of the wave angle and is especially useful in explicit time integration of the time-dependent wave equation.
4. The accuracy of the spectral element method is comparable to GLS and QSFEM methods, yet has the advantage of being able to be used for both time-harmonic (Helmholtz equation) and transient (wave equation) analysis. GLS and QSFEM have frequency (wavenumber) dependent coefficient arrays that don't lend themselves to transient analysis.
5. Optimal quadrature rules were derived for quadratic elements in one dimension and applied to nine-node bi-quadratic elements. The resulting spectral elements showed improved accuracy over standard Galerkin elements for plane wave solution oriented at different wave angles. A spectral element with lumped mass was also developed with improved accuracy than a Galerkin element with lumped mass.
6. Optimal quadratures were determined for eight-node tri-linear elements resulting in three-dimensional spectral elements with reduced dispersion error.

6.2 Future Work

The following items are suggestions for further extension of the ideas presented in this thesis:

1. Evaluate the accuracy of the spectral elements for non-uniform meshes and applications to exterior problems with non-reflecting and infinite elements.
2. Perform a transient analysis using both implicit and explicit time-integrators and compare accuracy of spectral elements with competing methods.

3. Further study the accuracy of the eight node tri-linear spectral element for three-dimensional applications.
4. Extend ideas of optimal quadrature rules for triangle and tetrahedral elements.

REFERENCES

1. Babuska, I.; Ihlenburg, F.; Paik, T.; Sauter, S.A. [1995]: A Generalized finite element method for solving the Helmholtz equation in two-dimensions with minimal pollution, *Comp. Methods Appl. Mech. Engrg.* 128, 325-359.
2. Babuska, I.; Osborn, J.E. [1983]: Generalized finite element methods: Their performance and their relation to mixed methods, *SIAM J. Numer. Anal.* 20(3), 510-536.
3. Bayliss, A.; Goldstein, C.I.; Turkel, E. [1985]: The numerical solution of the Helmholtz equation for wave propagation problems in underwater acoustics, *Comp. And Maths. With Appls.* 11, 655-665.
4. Belytschko, T.B.; Mullen, R. [1978]: On dispersive properties of finite element solutions. In: Miklowitz, J. (ed): *Modern problems in elastic wave propagation*, pp. 67-82.
5. Burnett, D. [1993]: A 3-D acoustic infinite element based on a generalized multiple expansion, submitted: *J. Acoust. Soc. Am.*
6. Goldstein, C.I. [1982]: A finite element method for solving Helmholtz type equations in waveguides and other unbounded domains, *Math. Comput.* 39, 303-324.
7. Hackbusch, W. [1992]: Section 4.7.2. In: *Elliptical Differential equations*, Springer Verlag, Berlin.
8. Harari, I. [1991]: Computational methods for problems of acoustics with particular reference to exterior domains. *Ph.D. Dissertation*, Stanford University, Stanford, California.
9. Harari, I.; Hughes, T.J.R. [1992]: Galerkin/least-squares finite element methods for the reduced wave equation with non-reflecting boundary conditions in unbounded domains, *Comp. Meth.. In Appl. Mech. Eng.* 98, 411-454.
10. Maccamy, R.C.; Marin, S.P. [1980]: A finite element method for exterior interface problems, *Int. J. Math. and Math. Sci.* 3, 311-350.
11. Mullen, R.; Belytschko, T.B. [1982]: Dispersion analysis of finite element semi discretizations of the two-dimensional wave equation, *Int. J. Numer. Meth. Engrg.* 18, 11-29.

12. Thompson, L.L.; Pinsky, P.M. [1994]: Complex wavenumber Fourier Analysis of the p-version finite element method, *Computational Mechanics*, 13, 255-275.
13. Thompson, L.L.; Pinsky, P.M. [1995]: A Galerkin least squares finite element method for the two-dimensional Helmholtz equation, *Int. J. Numer. Methods Engrg*, 38, 371-397.